Spring 2013

Development of a lumbar facet joint replacement

Amy Jo Criswell
University of Iowa

DEVELOPMENT OF A LUMBAR FACET JOINT REPLACEMENT

by

Amy Jo Criswell

A thesis submitted in partial fulfillment
of the requirements for the Master of
Science degree in Biomedical Engineering
in the Graduate College of
The University of Iowa

May 2013

Thesis Supervisor: Professor Nicole M. Grosland

Graduate College
The University of Iowa
Iowa City, Iowa

CERTIFICATE OF APPROVAL

_____

MASTER'S THESIS

_____

This is to certify that the Master's thesis of

Amy Jo Criswell

has been approved by the Examining Committee
for the thesis requirement for the Master of Science
degree in Biomedical Engineering at the May 2013 graduation.

Thesis Committee: _____
Nicole M. Grosland, Thesis Supervisor

_____
Tae-Hong Lim

_____
David G. Wilder

To Jameson and my parents

We gain strength, and courage, and confidence by each experience in which we really stop to look fear in the face…we must do that which we think we cannot.

Eleanor Roosevelt

ACKNOWLEDGMENTS

First, I want to thank my advisor Dr. Nicole Grosland. I would not be where I am without her guidance early in my college career. The insight and encouragement provided throughout the years has made me a better engineer. I am grateful every day for the opportunity that I got to work with her.

I would also like to thank my committee members for their input and suggestions. The time required to review and provide suggestions to me was immense and I am grateful. The knowledge that each member provides has improved my research study.

I am also grateful of the help that I have received from the MIMX laboratory members. I want to specifically thank Dr. Nicole DeVries and Dr. Nicole Kallemeyn for all the help they gave me while creating and running FE models. I also want to thank Dr. Anup Ghandi and Dr. Swathi Kode. Although my time with them was short, I gained an immense amount of knowledge from them.

I also want to thank my parents for their encouragement throughout the years. Their love and support has given me the strength to achieve my dreams and to never settle for an average life. They have made me so happy to be their daughter. Finally, I want to thank my fiancé, Jameson. Although he has challenged me throughout the years, he has made me a better person. I am so blessed to be able to call him my best friend and one day my husband.

TABLE OF CONTENTS

LIST OF TABLES

LIST OF FIGURES

CHAPTER 1

INTRODUCTION

1.1 Background and Rationale

Approximately 80% of the American population will experience back pain at some point in their lives [1]. Low back pain was cited as the most common type of pain according to a survey conducted by the National Institute of Health Statistics [2]. It has been estimated that back pain costs Americans approximately $50 billion each year [1]. These costs include health care costs and work time lost, however this statistic does omit other costs such as lost personal income and lost employer productivity due to medical leave. With the increasing amount of people experiencing pain, research is required to create solutions for patients with an already present state of pain.

Sources of low back pain include intervertebral disc degeneration, disc bulging/herniation, facet joint instability, spondylolisthesis, vertebral fracture, spinal stenosis and scoliosis [3, 4]. The first source, disc degeneration, has been a highly researched condition of the spine. A normal disc bulges in the posterior region with the nucleus pulposus shifted towards this region. A healthy annulus fibrosus is able to withstand high tensile loads. Overall, as long as the disc is hydrated and nourished, there should be no pain [4]. As people age a number of problems can occur. The disc begins to dehydrate and the fibers begin to experience fatigue failure [4]. As fibers begin to fail, the fibers may begin to press on the nerves which results in pain in the lower regions of the body.

The other region of the vertebra that contributes to low back pain is the facet joint. The facet joints may carry as much as 33% of the compressive load and also provide 45% of the torsional strength to each spinal unit [4]. As disc height decreases, loads and torsion may increase in the facet joint and cause deterioration leading to low back pain.

Dreyer and Dreyfuss estimated that low back pain is attributed to the facets in 15% to 40% of patients [5].

In the early stages of low back pain, doctors prescribe conservative treatments to alleviate symptoms. The first treatment is rest, analgesics and anti-inflammatory medicine [4]. Anti-inflammatory drugs and analgesics are used to relieve pain and rest alleviates any mechanical disruption to the spine. Continuing pain warrants use of medication and physical therapy. If this fails, surgical options are discussed.

Two methods used to study the effects of new solutions for treatment of spinal degeneration are finite element analysis (FEA) and mechanical testing. Due to cost and time constraints, the FEA approach is the more appropriate testing method for the early stages of implant development. Besides the benefits of cost and time, FEA creates a controlled and repeatable environment to test devices. FEA allows for determination of internal parameters (facet contact forces) that cannot be easily determined *in vitro* or *in vivo* without destroying the intact state of the spine. This method also allows for editing the model to generate healthy and diseased states of the lumbar to determine suitability of the device.

1.2 Project Aims

The overall objective of this study was to design a facet replacement system that could restore the normal kinematics in a degenerated lumbar spine. Specific objectives were to have alignment of the implant so that it does not disturb the kinematics of the vertebra and preserve the disc height of the functional spinal unit (FSU). Another objective was to build a "stop" into the implant to prevent subluxation and select a material based on the goals of the implant.

CHAPTER 2

BACKGROUND AND SIGNIFICANCE

2.1 Lumbar Spine Anatomy

The lumbar region comprises the lower portion of the spine. This area of the spine consists of five vertebrae which produces a lordotic curvature to the back. The lumbar spine carries the weight of everything superior producing a load of approximately 400 N [6]. Due to this large load and any vertebral degeneration, pain can occur which leads to the most common pain complaint among patients [5].

Each vertebra consists of a three-joint complex with the zygapophysial (facet) joint being two of them. Traveling caudally along the spine, the motion allowed at each level changes as the facet orientation changes. Due to the orientation of the articulating surfaces in the lumbar region, axial rotation (AR) is limited and a large amount of flexion, extension and lateral bending (LB) is allowed. Comparison between the facet orientations in each region is shown in Figure 1. The cartilage in the facet joints function to absorb compressive forces and provides the FSU ease of movement across the joint. The type of cartilage represented at the facet is hyaline cartilage which is hydrated by synovial fluid, thus classified as a synovial joint. Friction in the facet joint is low due to this fluid with a coefficient of friction of less than 0.002 [5]. The cartilage has no blood supply which signifies that the cartilage is unable to heal when damaged.

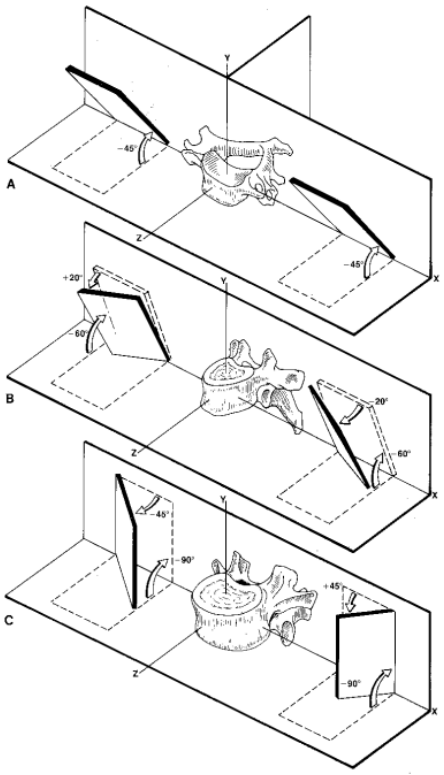

Figure 1: Facet orientation in cervical, thoracic and lumbar regions, respectively

Orientation of the fibers in the articular capsule is crucial in motion allowed in each region. The cartilage in the center of the joint has a fiber orientation that is parallel to the medial to lateral direction [5]. The orientation stabilizes axial rotation and allows for flexion and extension. The inferior region of the facet is thicker and more innervated than the other regions. This allows for the facets to resist compression but also results in back pain when the back is extended. The articular capsule is seen in Figure 2.

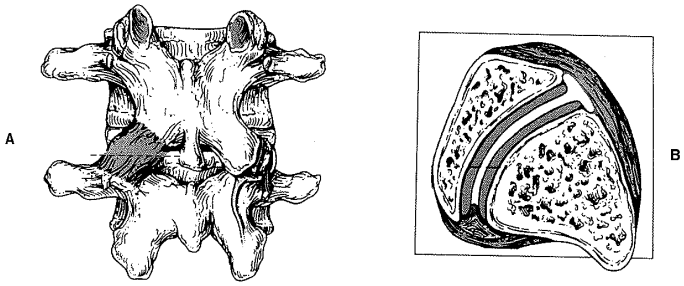

Figure 2: The posterior view of the facet joint (A) and the horizontal cross-section of the joint (B) [5].

The third joint in a FSU is the intervertebral disc. The function of this anatomic feature is to inhibit too much motion between segments but aid in the flexibility of the entire spine [5]. The disc is thicker anteriorly which helps create lordosis in the lumbar region. The disc has the ability to naturally regenerate but this function is weakened with injury and/or degeneration.

The disc is separated into two major areas: the annulus fibrosus and the nucleus pulposus. The annulus is a composite with embedded fibers in a ground substance arranged in several lamellae [5]. The anterior aspect of the disc is the strongest while the posterolateral is more likely to be injured. The fibers are arranged in an optimal manner to protect the disc during bending and torsion.

A diseased disc will first experience circumferential tearing. This tearing further weakens the structure and increases the likelihood that radial tearing will occur. Radial tearing connects the circumferential tears and the nucleus pulposus begins to protrude, causing disc degeneration. The nucleus pulposus is located more posteriorly in the lumbar region of the spine. It is avascular and absorbs most of the fluid in the disc.

The lumbar spine contains seven ligaments at each FSU. The anterior longitudinal ligament (ALL) is located on the anterior aspect of the vertebral bodies and discs [5]. The ligament is thicker from anterior to posterior at the body and fills the concavity created from the vertebra. The ligament limits extension and is thicker in the

lateral direction at the disc level which is unique to the lumbar region. On the posterior side of the vertebra is the posterior longitudinal ligament (PLL). This ligament resists flexion and helps prevent disc slippage on the posterior side. The PLL narrows at the body and thickens at the disc level, opposite of the ALL.

The remaining ligaments are found in the posterior region of the vertebra. The ligamentum flavum (LF) is attached to the right and left side of the laminae of adjacent vertebrae. This ligament supports the anterior aspect of the facet joint [5]. The interspinous ligament (ISL) connects the spinous process of each FSU. This ligament is responsible for limiting the last steps of flexion. Similar to the ISL, the supraspinous ligament (SSL) is located on the posterior aspect of the spinous process and limits the last steps of flexion. The intertransverse ligament (ITL) passes from the inferior side of the cranial transverse process to the superior side of the transverse process of the caudal vertebra. Like the LF, it supports the facet joint. The final ligament is the capsular ligament (CAP) which connects the articular processes of the facet joint. This ligament is responsible for limiting flexion and stabilizing axial rotation in extreme conditions [4].

The facets have been identified as a source of pain as early as 1976 [5]. With facet degeneration, it is common to experience disc degeneration at that level as well [4]. As disc degeneration progresses, the stresses are increased at the facets which propagates the degeneration at the facet location.

2.2 Lumbar Degeneration

2.2.1 Spinal Stenosis

The first type of degeneration is characterized as an increased pressure on the spinal cord caused by a narrowing of the spinal canal, called stenosis [5]. This can be a congenital or an acquired condition. A comparison of the two types of stenosis and a normal canal is shown in Figure 3. The space is compromised due to anatomic structures such as a displaced disc, osteophytes of the vertebral body or facet, hypertrophy of the

facet, joint inflammation or ligament invagination [4]. The primary cause of stenosis is arthrosis of the facet joint.

A symptom of spinal stenosis for most patients is pain when the lumbar spine is in extension. Patients find pain relief when flexing the spine. This is assumed to be from the reduction of invagination of the ligament, thus creating more space in the lumbar canal [4]. The neural and vascular elements will have a reduction in impingement due to the increase in space.

At the beginning of the disease, symptoms are similar to disc disease with low back pain and leg pain. Diagnosis of this type of degeneration is based on patient history, physical findings, electromyogram and radiographic evaluation [4]. Early stages of treatment include postural exercises, orthotics and epidural steroid injections. As the stenosis progresses, a more radical treatment may be required. This can include the removal of anatomic structures to relieve pain and create space in the lumbar canal.

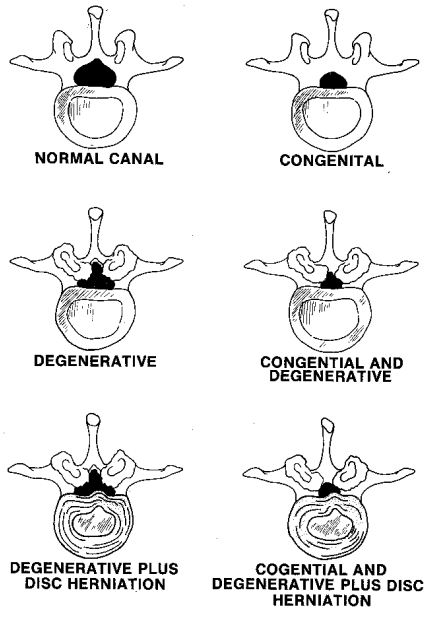

Figure 3: Normal canal and all the various spinal stenosis conditions [4].

2.2.2 Spondylolysis and Spondylolisthesis

Fracture of the lamina between the superior and inferior articular processes (pars interarticularis) is called spondylolysis [5]. One cause of this condition is due to fatigue failure of the spine. Due to forces through the facets and the spinous process, the combined stresses on the pars interarticularis causes fatigue and then fracture of the bone [4]. Other causes are improper formation of the vertebral arch, deterioration of the superior articular process or other conditions that cause improper bone formation of the posterior arch. Due to this defect, instability is created and the soft tissues at the FSU begins to plastically deform [4].

When spondylolysis is present, the vertebral body, pedicles, transverse processes and superior articular processes can displace anteriorly. This is a condition known as spondylolisthesis. As degeneration progresses, the superior articular processes begin to erode [5]. The vertebra that is superior to the facet degeneration begins to move anteriorly causing a stenosis of the canal. After failure of conservative treatments, the next step for patients is arthrodesis [4].

2.2.3 Osteoporosis

Osteoporosis is a disease characterized by below normal bone density. The low bone density is associated with the aging process and is more common in women during menopause. The average compressive force the vertebrae can withstand decreases by as much as 75% between the ages of 25 and 75 [7]. As the bone mass begins to decrease the strength of the vertebrae begins to decrease. In one study it was found that as bone mass decreased by 25%, the vertebral body's ability to resist spinal loads decreased by 50% [5]. When trabecular bone strength is less than the load applied vertebral fracture is more likely to occur.

2.2.4 Scoliosis

Scoliosis is defined by a lateral curvature of the spine. The condition can be found in any region of the spine, but the thoracic region is most commonly effected due to the length and central location of this region [5]. Causes of scoliosis include developmental and anatomic, such as hemivertebra (lack of development of one of the chondrification centers), or idiopathic [5]. With the presence of scoliosis, the anatomic features are no longer symmetrical about the sagittal plane and the spine has too much axial rotation in the wrong direction [4]. As the pain progresses decompression, corrections and arthrodesis are performed.

2.3 Current Surgical Treatments

Current surgical treatments for low back pain include: decompression, fusion across the diseased joint and a total disc replacement (TDR).

2.3.1 Decompression

Decompression is a surgical treatment that treats spinal stenosis. The procedure relieves pressure on the spinal cord or nerve root [4]. Decompression in the lumbar region is generally performed with a posterior approach. The types of decompression implemented in the lumbar region are vertebral body resection, facetectomy, laminotomy, laminectomy and any combination of the aforementioned. Facetectomy and laminectomy procedures will be discussed further.

2.3.1.1 Facetectomy

The first standard decompressive surgery to treat stenosis is a facetectomy. Along with removal of part or all of the facets, ligaments are resected. Depending on the type of facetectomy, partially or all of the interspinous, ligamentum flavum and capsular ligament are removed [8]. Based on *in vitro* results, a total facetectomy is not recommended due to the instability that is created in the spine [4]. Change in the joint

can lead to change in kinematics of the spine, which accelerates degeneration at adjacent levels [9].

2.3.1.2 Laminectomy

A laminectomy is a decompression method that partially or completely removes the lamina. Indications for this surgery occur when matter is impinging on the posterior side of the spinal cord [4]. In 2003, 2.1 per 1,000 enrollees in Medicare participated in a laminectomy procedure [10]. Goel reported that the failure rate of this type of surgical treatment can be as high as 48% and 10 to 20% of patients reporting a poor outcome [3]. Factors related to a good outcome of the surgery is: decompression on the nerve roots, minimal removal of facets to not create instability of the spine, early intervention before symptoms progress to paralysis, hard orthotics for three months and physical therapy of trunk muscles [11].

2.3.2 Fusion

Fusion is a surgical treatment that is prescribed to patients with an unstable spine [3]. This surgery eliminates motion at the surgical level(s). The procedure accounted for 47% of total spending for back surgery in 2003 [10]. Fusions treat the symptoms of low back pain, but not the disease that is producing the pain. A side effect of a fusion can be an increase in stress and motion in the adjacent segments to the surgical level [12]. The result is a high rate of complications due to the fusion. Leong et al. found that 52.5% of patients with a fusion had adjacent disc degeneration [3]. Spinal stenosis, increased motion and degenerative changes have been documented in the adjacent segments of a patient with fusion [4].

2.3.3 Total Disc Replacement

A motion preserving treatment for low back pain is a TDR. The use of TDR requires the partial removal of the disc. Typically, two metallic endplates are fixed to the

corresponding vertebral endplates and an articulating surface is inserted between the endplates to mimic anatomic motion [13]. The purpose of the implant is to restore the disc height as well as the biomechanics of the spine without altering the behavior of the adjacent segments. The future of this treatment is weary since the surgery itself is very difficult; exact placement is required for the surgery to be considered successful [12]. Due to this small tolerance, the learning curve for the procedure is longer. With degeneration of the discs, an increased load is produced on the facets which can lead to facet arthrosis [13].

Several studies have been conducted as to the effect of TDR on the spine. Demetropoulos et al. [14] studied the Prodisc-L prosthesis on the L3-L5 segment. The L4-L5 disc was replaced with the implant and the spine was rotated 10 Nm for F/E, LB and AR. The surgical level and adjacent level were evaluated based on range of motion (ROM), lordotic curvature and measured disc pressure for both intact and post-surgery.

At the L4-L5 FSU, flexion had no significant change but extension significantly decreased (from 2.2 degrees to 1.2 degrees) [14]. LB ROM did not significantly change while AR significantly increased. The angle of lordosis increased from 9.3 degrees to 12.2 degrees. The adjacent segment had minimal changes in ROM and disc pressure experienced no significant changes between intact and post-surgery.

Although the parameters that were evaluated yielded acceptable results, facet forces were not investigated. This is an important parameter to investigate further since it is known that changes in facet forces can lead to degeneration at adjacent levels.

Schmidt et al. [15] assessed the effect on facets and kinematics after the SB Charité III disc (Depuy Spine; Raynham, MA) was implanted into multiple levels. A FE model of the L1-L5 was created to accommodate multiple implantation configurations. With two levels implanted (regardless of configuration), the ROM for extension increased by 51% and flexion decreased by 5%. Facet loads increased by an average of 24%. Implantation of three devices increased extension by 69% and decreased flexion

11%. Four implants led to an increase of 91% for extension and a similar decrease of flexion as the case with two implants. Facet forces for three implants and four implants were increased by 11% and 8%, respectively.

Position of the implant also contributed to the success of the surgery. ROM was altered along with the observation of lift-off [15]. This phenomenon can lead to wear of the implant and eventually failure. It was determined that the more implants used led to greater amounts of kinematic changes.

Another treatment that has been suggested but not thoroughly investigated is a facet replacement. In a study conducted by King et al. [16], it was found that anywhere from 0 to 33 percent of the load is transferred to the facets depending on posture of the back. Another study developed by White and Hirsch [16] observed the role of the posterior elements in restricting motion. In the lower thoracic region, flexion/extension and lateral bending was increased by 15 percent and axial rotation had an increase in motion of 40 percent after posterior elements were removed. As stated earlier, it is common to have a coupling of disc and facet degeneration. A contraindication of a TDR is facet degeneration [12]. To remedy this, a facet implant design is needed.

2.4 Patent Review

Several solutions have been proposed to solve the problem of facet degeneration with an artificial facet. Discussed further are patents that have been developed over the past fifteen years.

2.4.1 Fitz: Artificial Facet Joint

One of the earliest designs was developed by William R. Fitz [17]. The patent details two components with a cone shape. It was designed to conform to each component's respective articular process and cover the entire surface. The inferior articulating surface has a low coefficient of friction to prevent resistance of motion at the

interface. The implants were designed to be attached to bone with fasteners. A figure of the implant outlined in this patent is shown in Figure 4.

Figure 4: Artificial facet developed by Fitz [17].

To insert this device, the articular processes do not have to be resected. The implant sits on top of the diseased facet, rather than replacing the entire facet. Due to this particular surgical procedure, the implant will not solve the issue of pain due to the presence of the diseased facets. Another disadvantage to the implant is the specificity of the design. In order to be inserted into a facet level, the implant would have to mate with the natural articular process. This creates a costly and time intensive manufacturing process to develop a patient-specific implant.

2.4.2 Goble et al.: Multiple Facet Joint Replacement

The next patent is a multiple facet joint replacement system shown in Figures 5, 6 and 7. It attempts to restore motion at the affected levels by removing the diseased facets and using a screw attachment at the pedicles of the vertebra [18]. The superior implant is attached to the cranial vertebra after removing the facets at the connection to the posterior

arch. Similarly, the inferior implant is fastened to the caudal vertebra by fasteners after the facet is removed at the connection to the pedicles.

The patent lists many alternative embodiments to replace one level of facets, multilevel replacement, or single facet replacement. The first embodiment in Figure 5 has one level of facets replaced.

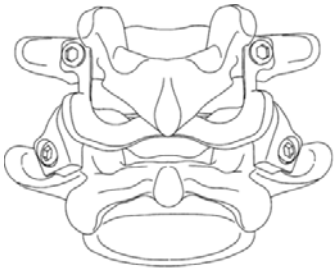

Figure 5: Single level replacement system [18].

Figure 6 and 7 illustrate the replacement of multiple levels and a single facet, respectively. The design features the ability to articulate with the natural facet. A disadvantage of this particular design is the use of screws for attachment. With cyclic loading and any bone degeneration at the attachment site there is a risk of screw pullout, thus implant failure.

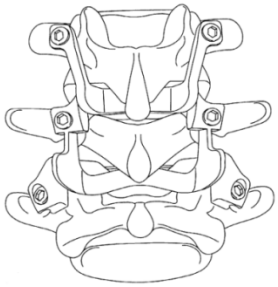

Figure 6: Multi-level replacement system [18].

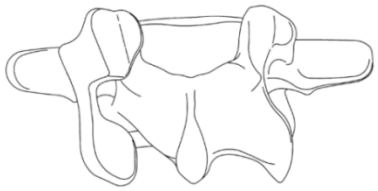

Figure 7: Single facet replacement [18].

2.4.3 Reiley: Facet Arthroplasty Devices and Methods

The goal of this patent was to create an implant that avoided common problems for treatments of the spine [19]. Such problems include increase in spine stiffness, increased loads on adjacent levels and predictable high failure rates. The implant was designed to have the versatility to replace levels spanning T11 through S1.

The caudal facet was designed to be fixed near or to the pedicles of the corresponding vertebra. The cranial implant is to be fixed to the vertebral body. This includes the pedicle, lamina, spinous process or any combination of the aforementioned. Both implants are shown in Figure 8. The implant was designed to reduce or eliminate the occurrence of spondylolisthesis and create a desired articulation that mimics the anatomic motion.

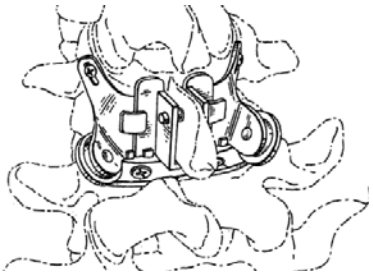

Figure 8: Facet arthroplasty device designed by Reiley et al [19].

Figure 9 and 10 illustrate a superior view of different embodiments of the caudal prosthesis. Figure 9 has a ball-shaped articulating surface and is fixed to the vertebral body by pedicle stems. Figure 10 has a similar geometry as Figure 9 but is attached to the body by pedicle screws.

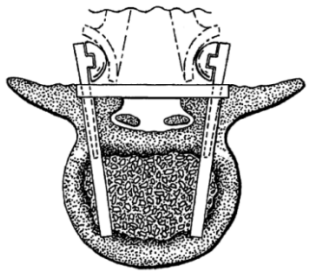

Figure 9: Caudal prosthesis attached by pedicle stems [19].

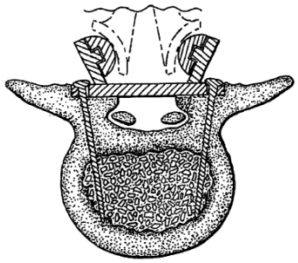

Figure 10: Caudal prosthesis attached by pedicle screws [19].

The disadvantage of this system is the implant requires a complicated surgical process. Multiple attachment sites and deep drilling creates a difficult surgery for the surgeon. A more simple prosthesis will be more ideal for the surgeon.

2.4.4 Goble et al.: Facet Joint Replacement

The next patent is a continuation of the Multiple Facet Joint Replacement patent developed by Goble et al. [20]. The cranial vertebra facets are resected at the posterior

arch junction and the prosthesis is fixed to the bone with a press fit fin. As with other facet implant patents, the caudal vertebra is resected at the pedicles and a press fit post is inserted into the bone. The bone is to be prepared with a broach or punch.

Another embodiment of the prosthesis is an implant with a flange that is attached to match the orientation of the natural facet. Shown in Figure 11, a fastener is used to fix the implant. The implant has the ability to be porous coated to promote bony ingrowth. A design feature of the implant is the ability to just replace the diseased or compromised facets. Similar to the original patent, the embodiment that utilizes screws has the potential for screw pullout with bone deterioration and cyclic loading.

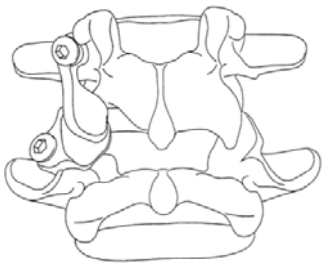

Figure 11: Single facet replacement [20].

2.4.5 Hudgins et al.: Facet Replacement/Spacing

The facet replacement/spacing and flexible spinal stabilization developed by Hudgins et al. [21] attempts to solve the problem of degenerated facets. To implant this device, the diseased facets are removed. The first embodiment, Figure 12, is a band that secures the two vertebrae and is fixed to the two vertebrae. This implant provides a restraining force against the motion of the two vertebrae.

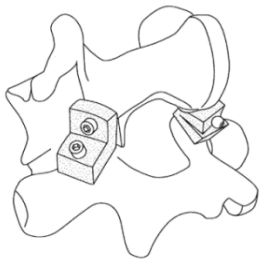

Figure 12: Band replacement device developed by Hudgins et al [21].

The second embodiment is shown in Figure 13. The facets are removed in a similar manner as with the first embodiment. The prosthesis includes an articulating surface, spinous process spacer and anchoring element. The facet is replaced with the articulating surface and this element is attached to the spacer by a flexible connecting member. The spinous process spacer stabilizes the implant while it is anchored to the superior vertebra by a flexible anchoring element.

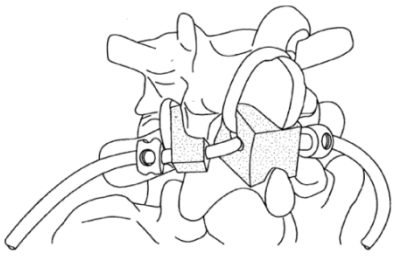

Figure 13: Second embodiment designed by Hudgins et al [21].

The first embodiment eliminates normal kinematics of the spine since it acts more like a fusion device. An objective of the current research is to design a device that returns the kinematics of the spine. The second embodiment is a complicated design that would require a complicated procedure. The ability to implant this device would have a large learning curve for most surgeons inexperienced with this type of procedure.

2.4.6 Krishna et al.: Posteriorly Inserted Artificial Facet

The facet prosthesis described in the current patent details the ability to work with the described disc implant as a single unit [22]. The artificial facet is attached to a superior disc and an inferior disc. One member of the implant is telescopically mounted into the mating implant, shown in Figure 14. The unit also has the ability to be fixed to the vertebral body by pedicle screws right above and below the disc, without the use of an artificial disc. The design allows for flexion, extension and lateral bending but very little in axial rotation.

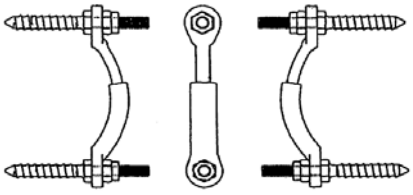

Figure 14: Facet prosthesis designed by Krishna et al [22].

The disadvantage of the prosthesis is similar to past implants using fasteners that attach to the vertebral body. With any osteoporosis of the bone, the screw may loosen and the implant would fail.

2.4.7 Stone et al.: Facet Replacement Device Removal

Stone et al. [23] designed an implant that requires the removal of the spinous process and attaches the superior implant to the pedicle. The inferior portion of the implant removes the diseased facet and articulates with the superior portion through a type of "ball and socket" joint, shown in Figure 15.

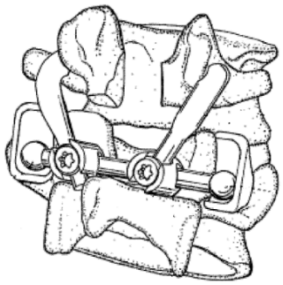

Figure 15: Ball and socket facet prosthesis [23].

The surgical procedure requires a laminectomy which exposes the spinal cord and can lead to damage [24]. The project proposes an implant that will attach at the pedicle and will not require removal of the spinous process.

2.4.8 Chin et al.: Dynamic Facet Replacement System

Chin et al. [25] designed an artificial implant to replace the inferior facets and the superior facets. It also removes the entire facet joint in between the inferior and superior facet removal. The purpose of this is to connect the two articulating surfaces with the surfaces of the inferior and superior surfaces. The goal of the design is to restore spinal stability and mobility.

The design is limited to a multilevel replacement as seen in Figure 16 (exploded view of implant shown in Figure 17) [25]. When degeneration is located at a single FSU, the patent design is replacing healthy joints. The current study's goal is to create a single-level replacement system.

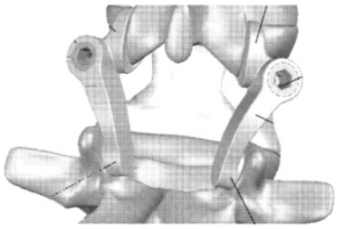

Figure 16: Dynamic facet prosthesis developed by Chin et al [25].

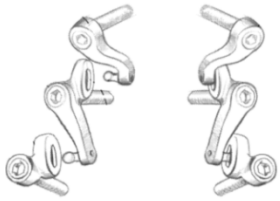

Figure 17: Exploded view of the dynamic facet replacement system [25].

2.4.9 Kwak et al.: Facet Joint Prosthesis

Kwak et al. [26] designed a facet implant that has a superior component which is an elongate member and an inferior component that mates with the elongate member. The system is shown in Figure 18.

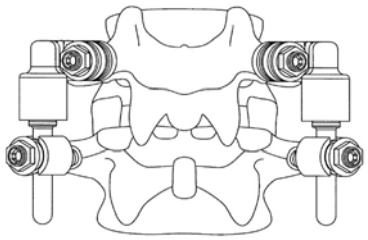

Figure 18: Facet joint prosthesis designed by Kwak et al [26].

The rod translates relative to the housing unit. Due to this, the design allows flexion, extension and lateral bending but resists anterior/posterior shear and axial rotation. There is an optional cross-connector for further stabilization shown in Figure 19.

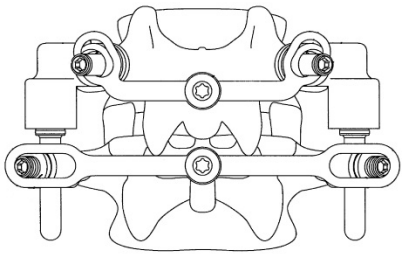

Figure 19: Prosthesis with connector [26].

Issues with this design include the difficulty in using minimally invasive surgery. During the procedure, a larger cut may be required in order to mate the two components. The design proposed for the current research does not include complicated structures that complicate surgery.

2.4.10 Link: Facet Joint Prosthesis

Link [27] developed a patent for a facet joint implant that can be inserted into any region of the spine. A bearing piece and a guide rod are assembled and the bearing piece contains a pressure plate that is supported by the vertebra, shown in Figure 20. In order to be placed throughout the spine, a pivot joint has been integrated into the design. The joint allows for movement in the coronal and sagittal plane. Another feature of the prosthesis is the telescopic rod to adjust the implant for different vertebra thicknesses. The implant also has the ability to articulate with the natural facet.

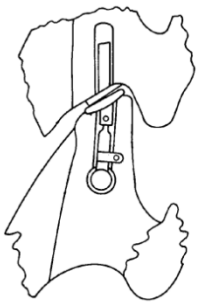

Figure 20: Facet joint prosthesis for the cervical vertebra [27].

Due to the versatility of the implant, the design has a pivot joint to be implanted in any region. Once implanted, the surgeon has to secure the implant from twisting and changing the kinematics at that FSU. Although the inventor designed teeth on the bearing plate, the teeth may not be enough to secure the entire implant. The design that is proposed for current research is only implanted in the lumbar region.

2.4.11 Kwak et al.: Artificial Facet Joint

DePuy Spine, Inc developed a patent titled Artificial Facet Joint [28]. The patent describes two embodiments of the design shown in Figure 21 and Figure 22. The superior portion of the device is the bearing element of the implant and is rotatable with an opening for attachment of a rod. The inferior implant includes an extension rod that fits in the bearing element of the superior device.

The implants were designed to have a variety of configurations and can replace other posterior elements besides the facets. These include posterior ligaments, lamina, etc. It was also a goal of the design to be able to use the implants with a TDR. Issues taken with the design include the lack of motion in lateral bending and axial rotation. The motion that is preserved is flexion and extension. Another issue is the laminectomy required to insert the device. Stated earlier, this could lead to spinal cord damage.

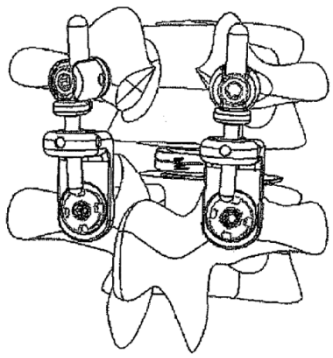

Figure 21: An artificial facet joint designed by Kwak et al. [28].

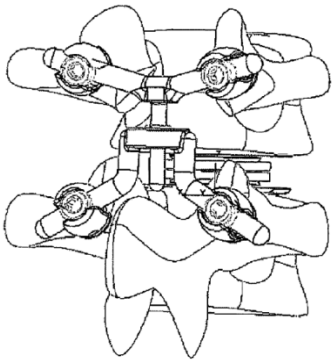

Figure 22: A second embodiment with the connector as a Y shape [28].

2.5 Analysis of Facet Joint

2.5.1 Finite Element Modeling and Mechanical Testing

Many research groups have dedicated their time to determining the importance of the facet joint in the kinematics of the spine. One method that has been utilized is mechanical testing. Though this leads to insightful results, the technique has been criticized due to the disruption of the facet joint which leads to inaccurate results. Another tool developed to evaluate the joint has been finite element modeling. Both techniques are discussed further.

Kuo et al. [29] developed an asymmetrical L1-L5 FE model with CT slices at 1 mm increments. A sterolithography (STL) surface was created with 3D-DOCTOR software and smoothed with PATRAN. Mesh generation and processing was completed with ABAQUS (Ver. 6.5-1). Posterior bone, trabecular bone and ground substance were modeled as 4-node linear tetrahedral elements (C3D4) instead of hexahedral elements (C3D8). Ligaments, cortical shell, endplates and annulus fiber were modeled as 3-node triangular membrane elements (M3D3). The facet contact definition had a coefficient of friction of 0.1. Two different types of models were run. The first was a model with only a compressive load applied at 300 N, 460 N or 600N. The second model had a preload similar to the first model followed by moments starting at 5 Nm and incrementing by 5 Nm to 20 Nm for F/E and axial rotation. Load and moments were applied to the superior side of the L1 vertebral body and the inferior side of the L5-S1 endplate was held rigid.

Intradiscal pressure, von Mises stress/strain and facet forces were calculated. The latter is the component most relative to this report. The researchers found that the moments influenced facet forces more than a change in preloads. Also, asymmetric facet forces were calculated. This is believed to be due to the asymmetry of the surface or manual editing errors. The asymmetry becomes more evident as the moment increases as opposed to an increasing preload.

Cook [30] and Cheng [31] developed models to study the facet joint gap without violating the integrity of the joint. Fiducial markers were attached to the bodies of L1-S1 specimens with an adhesive before CT scans were taken. Cook assigned a threshold of 3 mm for the region of interest (ROI) based on the assumption that the cartilage is 1 mm thick on each side with a gap of 1 mm in the neutral position. A ROI as defined by Cook is “the facet and surfaces within a threshold distance from the surface of the neighboring vertebral body.” Specimens were cleaned and potted at the L1 and sacrum. Testing protocol required testing of the specimen in load control with three cycles of F/E with a sinusoidal load profile of 0.01 Hz and amplitude of ±7.5 Nm. Lateral bending load was

held at zero and axial rotation was fixed to zero rotation. Trackers were monitored with the Optotrak 3020 motion capture system (Optotrak, Northern Digital Instruments, Canada).

The mechanical testing results were registered to the solid-body model. A contact area ratio (CAR) was calculated as the number of vertices in the ROI at that time point to the number of vertices that constitute the facet surface. CAR proved to be sensitive enough for the test to show differences between flexion and extension. Results point to an ability to measure differences between vertebral levels which helps with further development of surgical techniques and implant devices.

Cheng et al. [31] followed Cook's research with his own study to calculate minimum distance (MD) between the ROI of a particular facet joint. Six specimens were potted at the T12 and S1 and markers were attached using a similar method as Cook. After CT scans, the specimen was mechanically tested following the same protocol as Cook with additional tests of lateral bending and axial rotation. The frequency of the sinusoidal load profile was lowered to 0.005 Hz but the amplitude remained the same. After testing of the intact model, pedicle screws with a rigid rod were attached at the L3-L4 level and tested with the same protocol as the intact model. Similar methods to Cook's study were used to create a rigid body model.

MD was used to indicate changes that occurred throughout ROM and different facet states. Cheng determined that the new method is more precise in determining lumbar properties than more traditional approaches such as ROM, neutral axis and helical axis motion. It was the goal of the researcher to be able to better develop medical devices with this new information.

Sawa and Crawford [32] tested several T12-L2 specimens with custom gages to determine facet loads. Markers were attached to guide wires which were inserted into the posterior portion of the vertebra, trying to avoid the lamina. Pure moments of 7.5 Nm were applied to F/E, AR and LB. After stiffness testing, L1 and L2 were disarticulated

and examined for degeneration. Strain gages were then calibrated after testing with known loads.

Models were later created of each tested specimen with the use of NeuralWorks Predict (Neuralware, Carnegie, PA). This was completed with the results from the calibrated strain and load data. Facet load characteristics of magnitude and location were determined from the models. The accuracy of the model was measured by comparing the model's calculated load and location to a known applied load.

Results indicated that the loads, from largest to smallest, were the contralateral facet during AR, extension, flexion, LB and finally the ipsilateral facet during AR [32]. Addition of a follower load increased extension forces. During the flexibility tests, the locations of mean load had no statistical change in direction. After reviewing literature results, other groups have consistently listed facet loads as higher in AR than in extension, matching this study's results. Further, the accuracy of the strain gauges is measured to be between 3 to 15% with a graphical solution. It was determined that this method of testing is effective for calculating facet loads.

Sharma et al. [33] created a FE model of the L3-L4 FSU to demonstrate the nonlinearity of facet contact. Four models were developed with different facet parameters. The normal model represents values reported in literature. The other three cases had the gap and orientation angles differ from the normal case. Another model was created with a 100% bilateral facetectomy to study the effects of facet removal. To model a nonlinear facet behavior, an Incremental Updated Lagrangian approach was used.

The model was tested in compression, 6 Nm extension moment and 6 Nm torsion moment [33]. Percentage of load transmission did not change very much between cases. When the gap was changed from 0.6 mm to 0.05 mm, the facets carried 14% more of the load during extension. When subjected to torsion, the percentage of load transmission increased by 38.9% from normal to a smaller gap. Altering the facet orientation changed

loads transferred through the facets for both extension and torsion, however it was not nearly as large of a change as when the gap was modified. When determining importance of the entire facet on the disc, removal caused large strains to incur during large rotations.

2.5.2 Implant Testing

Several implants have been mechanically and computationally tested to determine quantitatively of the ability to restore kinematics of the spine. Wilke et al. [34] first looked at biomechanics after replacement of the posterior portion of the vertebra with the TOPS system (Impliant Ltd., Ramat Poleg, Israel), seen in Figure 23. The posterior dynamic system is constructed of two endplates with a polycarbonate urethane boot. Pedicle screws are attached to rods that connect to the superior and inferior endplates. To complete *in vitro* testing, a bilateral laminectomy with a facetectomy of the inferior facets of the L4 had to be performed to implant the device. A unique flexibility testing setup was developed that held the caudal end fixed in the apparatus and the cranial end mounted to a gimbal. The motion was unconstrained in all degrees of freedom. The spine was subjected to pure bending moments of 7.5 Nm for intact, degenerated and implanted spine.

Wilke et al. [34] measured the quality of the implant by calculating and statistically comparing ROM and intervertebral disc pressure of the intact, the degenerated spine and the spine with a dynamic device. The implant restored the defected ROM to intact levels. Most of LB and AR was restored while 85% of intact motion was restored for F/E. The results of the disc pressure demonstrated that the implant restored pressure to near intact levels. This suggested that the implant is able to carry a percentage of the load.

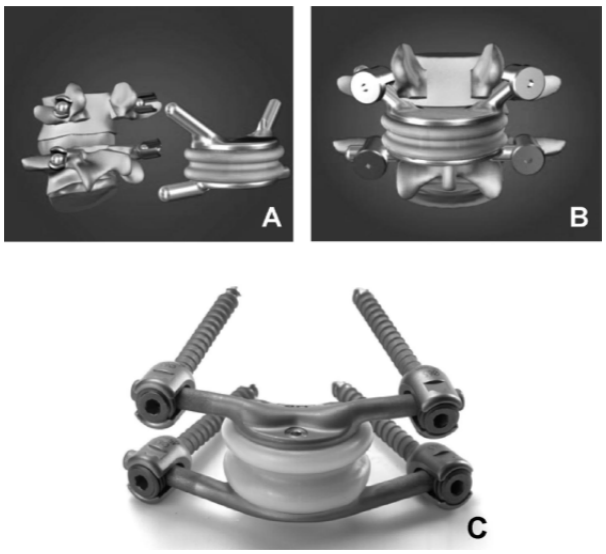

Figure 23: TOPS diagrams and posterior view [34].

Other research groups have looked at different posterior dynamic replacement systems. Zhu et al.[24] and Phillips et al. [35] studied the Total Facet Arthroplasty System (TFAS; Archus Orthopedics, Redmond, WA). This device is designed to allow 15 degrees of F/E, 14 degrees of combined right and left lateral bending and a combined 4 degrees of left and right axial rotation. Similar to Wilke et al., the ROM was used to classify the success of the implant in both studies. Both groups also looked at helical axis of motion for further kinematic evaluation of the system. Phillips et al. [35] further evaluated the load-displacement curve by calculating and comparing the neutral zones of the intact and the operated level. This group also looked at ROM of adjacent levels and quality of motion at these levels as well as the operated level. The mechanical testing setup is depicted in Figure 24.

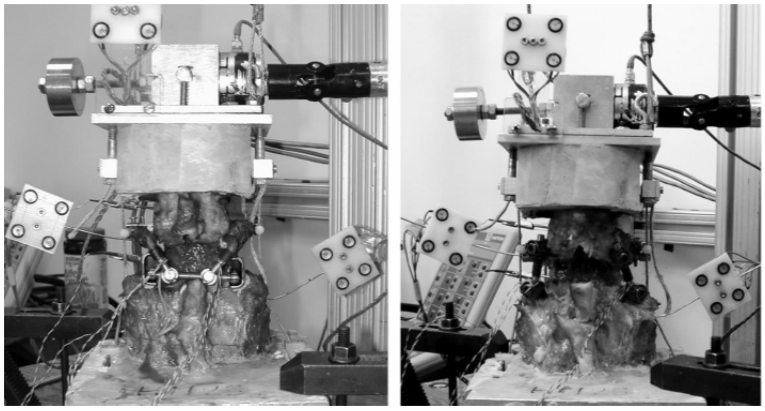

Figure 24: Mechanical set-up of the TFAS [24].

Similar testing set-ups were constructed by both groups. Both reports found that the ROM at the operated level was not significantly different from intact values. Reported by Zhu et al [24]., TFAS restored motion to 81% of intact in flexion, 68% of intact in extension, 128% of intact in axial rotation and 88% of intact in lateral bending. In flexion and extension, the helical axis of motion was restored to intact levels for both studies. Lateral bending was also restored in Zhu et al. research but axial rotation was significantly increased from intact levels. Stated earlier, Phillips et al. [35] also looked at the neutral zone of operated level and motion at the non-operated levels. The neutral zone was defined as the difference in the FSU angle between the loading and unloading curves at 0 Nm bending moment. The implant restored F/E at adjacent levels to intact, although L2-L3 level was significantly higher than intact. This was believed to be due to a partial laminectomy of the L3. Overall, the TFAS restored motion to intact levels but due to significant differences in axial rotation, further evaluation is warranted.

Goel et al. [36] created a L3-S1 model and mechanical test to study the Anatomic Facet Replacement System (AFRS; Facet Solution Inc, Logan, UT) on the biomechanics of the spine. For the FE study, the facets were removed at the L4-L5 level and the system was attached to the spine by pedicle screws. The inferior side of the S1 was held fixed

and loads and moments were applied to the superior end of the L3 vertebra. The FE model that was used for testing is shown in Figure 25. Testing protocol followed in this experiment was similar to previous groups discussed throughout this report.

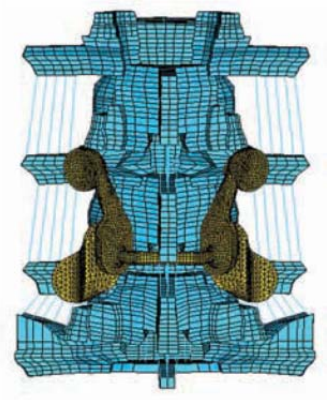

Figure 25: FE model of spine with AFRS implanted at L4-L5 FSU [36].

Results indicated the implant restored motion to intact levels. Extension was 82% of intact motion, flexion was 103% of intact flexion, lateral bending was 82% of intact lateral bending and axial rotation was 15% less that intact axial rotation [36]. The FE model and mechanical tests results agreed with respect to ROM. Other kinematic values were calculated. Intradiscal pressure was close to intact pressure with the implanted device. A new parameter that other groups did not investigate due to the lack of a FE model was facet loads. The facet loads of the spine with the implanted device compared well to the loads of an intact model for extension and axial rotation. An issue that was noted was the pedicle screws used for fixation of the implant. High stresses were calculated at the bone-screw interface. Further long-term testing is required to determine effect of these stresses and whether a reduction of stresses is needed to improve longevity of the device.

Panjabi et al. [37] tested the StabilimaxNZ (Applied Spine Technology, New Haven, CT) system to determine if dynamic implants are a better option than fusion for unstable spines. Flexibility test and hybrid mechanical tests were performed on six T12-S1 specimens. Decompression was simulated followed by implantation of the dynamic device. Besides ROM, the average adjacent-level effects (ALE) were measured. The implant reduced F/E to 62.4% of intact motion for the flexibility test. Lateral bending decreased motion to 57.5% of intact lateral bending and axial rotation increased motion. At the adjacent level (L3-L4) the ALE was reduced by one-half for F/E and one-sixth for both lateral bending and axial rotation compared to the fusion experimental results. It was determined that the system reliably stabilized the spine for flexion-extension and lateral bending but not axial rotation.

The last implant system was the Auxiliary Facet System (AFS; Clariance Spine, Saint Ismier, France) evaluated by Charles et al [38]. An experimental setup is shown in Figure 26. The goal of the device was to preserve flexibility but add stability to the entire spine. The device can be implanted at multiple levels with a pedicle screw fixation. The mechanical testing measured ROM, intradiscal pressure and mean center of rotation.

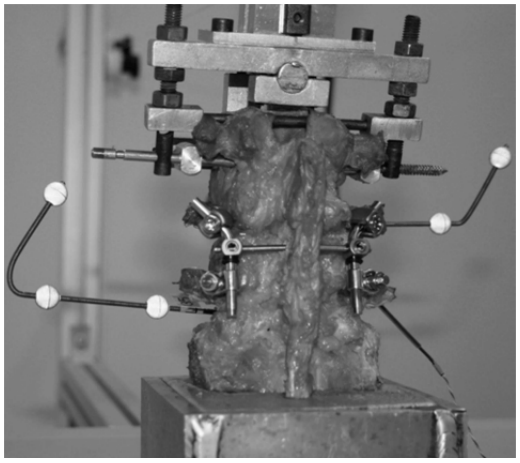

Figure 26: AFS experimental setup [38].

Flexion-extension of the implanted spine was 86% of intact F/E. Lateral bending of the lesion created spine was corrected to close to intact levels with the implanted system. Axial rotation with the implanted device decreased motion significantly (only 53% of intact motion) from the intact values. The motion decreased more when the device was implanted and a facetectomy performed (38% of intact motion). The reduced motion is thought to be caused by the stabilizing cross-link member of the implant. The mean center of rotation had a similar area to the intact state and intradiscal pressure suggested pressure was limited by the implant.

CHAPTER 3

IMPLANT MODELING

3.1 Introduction

The proposed implant was designed to be inserted at the L4-L5 level to replace the resected facets. To design an implant that surgeons would find useful, it was determined that a simple device was required. Consequently, a "ball and socket" style joint was created based on the simplicity and success of other artificial joints that use this design (i.e., hip replacements).

Three different models were created with the first design iteration of the implant being discarded early in the design process due to high likelihood of failure. The second iteration was designed to be more conforming than the first design to prevent implant fracture at the articulating surface. A third iteration was proposed to look at differences between geometries of the implant with the second iteration. Stresses of the second and third iterations were compared after a compression test was performed.

3.2 Pro/E Modeling

3.2.1 Design Iteration I

Dimensions of the L4-L5 facets were determined from literature references. Facet cartilage is approximately 0.2 mm thick with a gap at the facet of 0.4 mm [15]. Facet height and width were approximated by Meijer et al. [39] as 16.7 mm and 14.7 mm, respectively. Angles of the facet were reproduced by alignment of the implant relative to the vertebra.

The inferior component was designed in Pro/Engineer Wildfire (Version 4.0, Parametric Technology Corporation). A rectangular sketch with two of the corners rounded was extruded 6 mm to create the base of the implant. The base was mirrored about the mid-plane since one-half of the base was sketched due to symmetry (Figure 27).

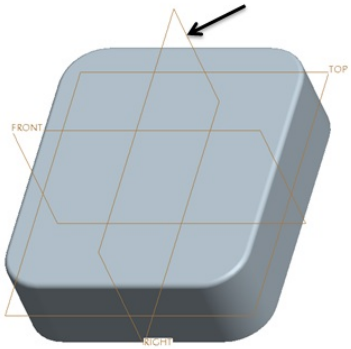

Figure 27: Datum the base part was mirrored about.

After the base was extruded, a post was added on the inferior side of the component for fixation to the vertebra (Figure 28C). The component was designed to attach to the pedicle region of the inferior facet by press-fit. Other inventors of facet replacement system had discovered the pedicle to be a better fixation site due to low variability between patients compared to the posterior arch [18]. On the superior side of the component, an articulating surface was created. The feature was a semi-circle that mates with the surface of the superior prosthesis (Figure 28A and 28C). The articulation does not follow the entire length of the implant due to the objective of building in a "stop" to prevent subluxation of the two components. Rounds were created on sharp corners of the mating side of the implant. The final implant design of Iteration I is illustrated in Figure 28.

The base of the superior component was created with the same technique as the inferior prosthesis with a 7 mm thickness. A spike was designed to extend off the base in the superior direction. The superior component attaches to the pedicle region of the caudal vertebra, similar to the inferior component. On the side that mates with the inferior component, an articulating feature protrudes from the base of the implant. At the end of the protrusion is a spherical feature for smooth articulation. The implant is shown in Figure 29. The two components articulate with each other through a "track" system

(Figure 30). This design allows for flexion/extension of the lumbar vertebrae but restrains rotation.

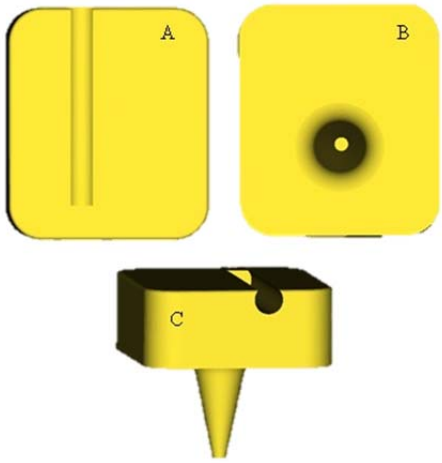

Figure 28: The anterior (A), posterior (B), and lateral (C) views of the Design Iteration I inferior component.

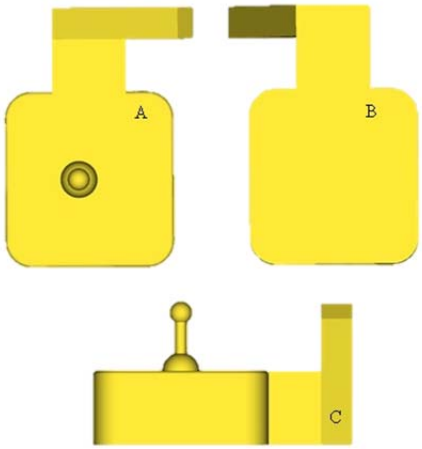

Figure 29: Anterior (A), posterior (B) and lateral (C) views of the Design Iteration I superior prosthesis.

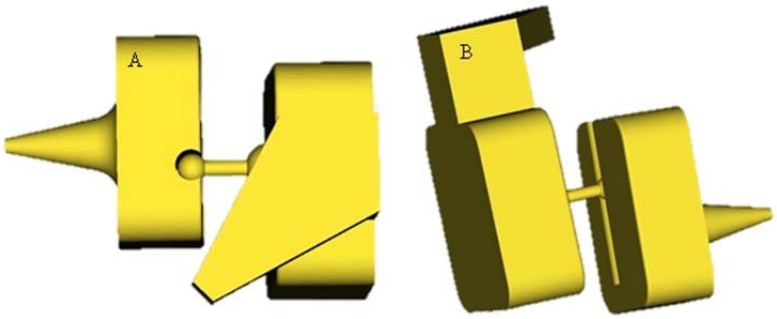

Figure 30: Superior (A) and isometric (B) view of the inferior and superior components constructed together.

3.2.2 Design Iteration II

After investigating the magnitudes of loads transferred through the facets, a new design was proposed. The implant was designed to be more conforming to allow for a better transfer of stresses at the articulating surfaces.

The inferior component utilized the same base design as Design Iteration I. The base was further extended to 7 mm and mirrored about the right datum. The base thickness was increased to compensate for the added gap between the superior and inferior components when the peg was removed from the superior component. The same post was added to the posterior side of the component (Figure 31B). A more conforming articulating surface was added to the anterior side of the device (Figure 31A and Figure 31B). The feature is much deeper than the previous version's articulating surface and still allows flexion and extension. The surface still has the ability to limit axial rotation. Design Iteration II inferior component is shown in Figure 31.

The superior prosthesis is the same base part as the inferior component with an added 1 mm to the base compared to Iteration I design. Similar to the inferior component, the addition of 1 mm was to accommodate for the missing peg on the superior component for the second design iteration. The post is exactly the same as the previous version. The articulating surface was created to sit closer to the inferior

component. The views of the superior component are shown in Figure 32. The two mating components are shown together in Figure 33.

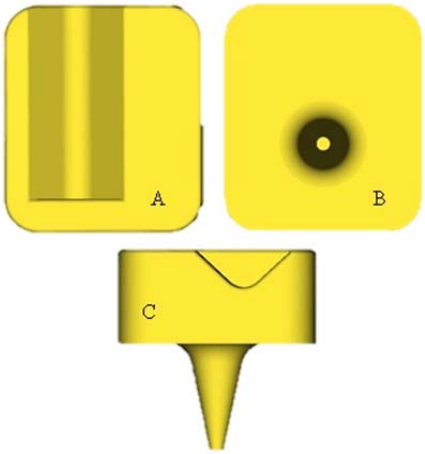

Figure 31: The anterior (A), posterior (B), and lateral (C) views of the Design Iteration II inferior component.

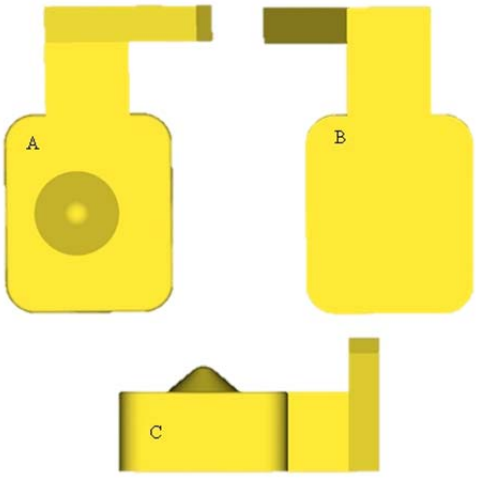

Figure 32: Anterior (A), posterior (B) and lateral (C) views of the Design Iteration II superior prosthesis.

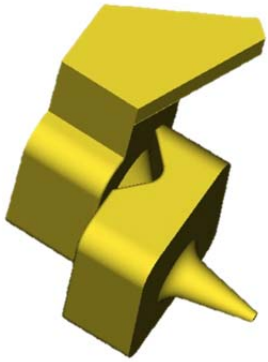

Figure 33: An isometric view of the superior and inferior components when inserted together.

3.2.3 Design Iteration III

The articulating geometry of the second iteration was altered for comparison of the stresses with different articulating geometries. The inferior component had a similar conforming design feature as Design Iteration II. The articulating surface shown in Figure 34 was created to be more spherical as opposed to the wedge shape of the previous design.

The superior component has an added curve feature to the once flat part of the device. This was to allow for a more "rocking" motion of the implant relative to the inferior component. The articulating surface was also redesigned to be more spherical to better transfer stresses from the superior component to the inferior component when loaded. Multiple views of the superior component are shown in Figure 35. Figure 36 shows the device as it would appear implanted in the spine.

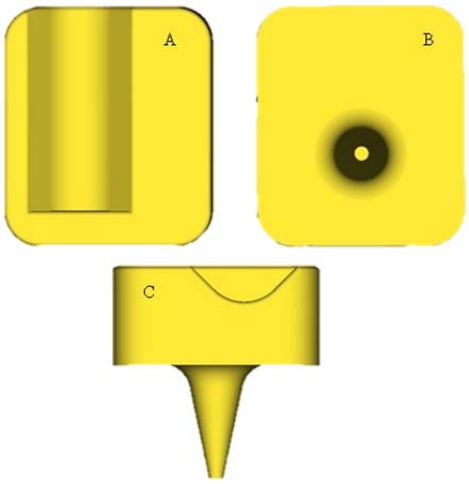

Figure 34: The anterior (A), posterior (B), and lateral (C) views of the Design Iteration III inferior component.

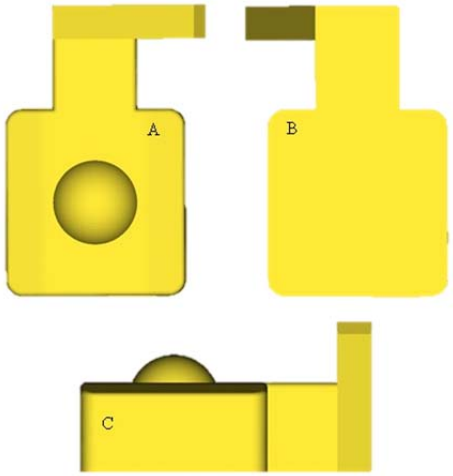

Figure 35: Anterior (A), posterior (B) and lateral (C) views of the Design Iteration II superior prosthesis.

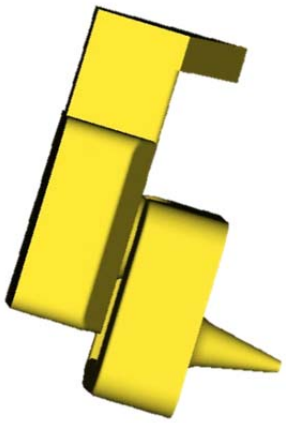

Figure 36: An isometric view of the superior and inferior components mated.

3.3 Finite Element Modeling

3.3.1 Compressive Loading

3.3.1.1 Methods

After completion of the Pro/E models, an STL was created of each component to be used for mesh generation. Pre-processing was completed with an open-source software package called IA-FEMesh (Iowa-FEMesh; www.ccad.uiowa.edu/MIMX/projects/IA-FEMesh) [40]. Building blocks were constructed around the individual components to generate an optimal FE mesh. FE meshes of the Design Iteration II right inferior and superior components are shown in Figure 37 and Figure 38, respectively. The second iteration's right inferior component was 4,400 elements and the superior right component was 2,712 elements. Design Iteration III was composed of 4,100 elements and 2,900 elements for the right inferior and superior components, respectively (Figure 39 and Figure 40).

Eight-node hexahedral elements were used for the inferior components. A metal-on-titanium (elastic modulus, E =110 GPa, Poisson's ratio, ν=0.32) design was tested along with a metal-on-poly design (E = 900 MPa; ν=0.3) [41]. The superior component was modeled as rigid elements.

Figure 37: A final mesh of the inferior component for the Design II iteration.

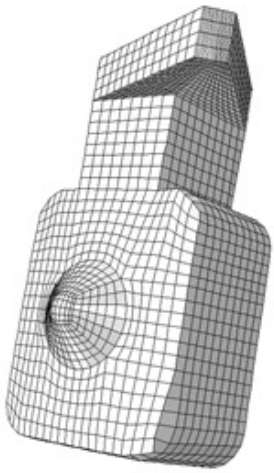

Figure 38: The Design II iteration's superior component final mesh.

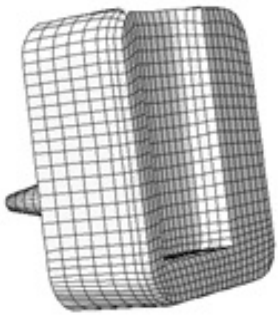

Figure 39: Design III inferior mesh.

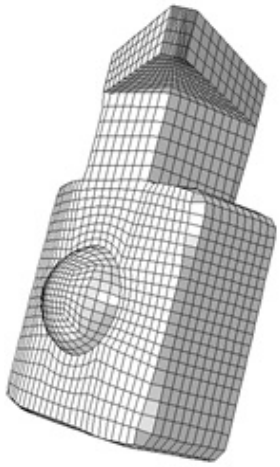

Figure 40: Third iteration superior component mesh.

A surface-to-surface contact definition was simulated with appropriate coefficients of friction (poly, μ= 0.14; titanium, μ= 0.30) [41, 42]. Surfaces of the flat part were considered to be in contact, along with the articulating surfaces of the superior and inferior component.

The posterior side (i.e. the side of the implant to be attached to the pedicle of the L5 vertebra) of the inferior component was held rigid so no translation could occur in the x, y and z direction. A reference node was positioned at approximately the center of the non-articulating side of the superior component.

Before a compressive force could be loaded on the implant, the superior component had to come into slight contact with the inferior component. A minor amount of displacement in the x and y direction of the superior component was applied with a small rotation about the z axis (Figure 41). A compressive load of 350 N was applied to the posterior side of the superior component, normal to the surface (Figure 42) [29, 32]. All other translations and rotations were held at zero during this loading step. The final step was to release boundary conditions of zero translation and y and z rotation of the superior component.

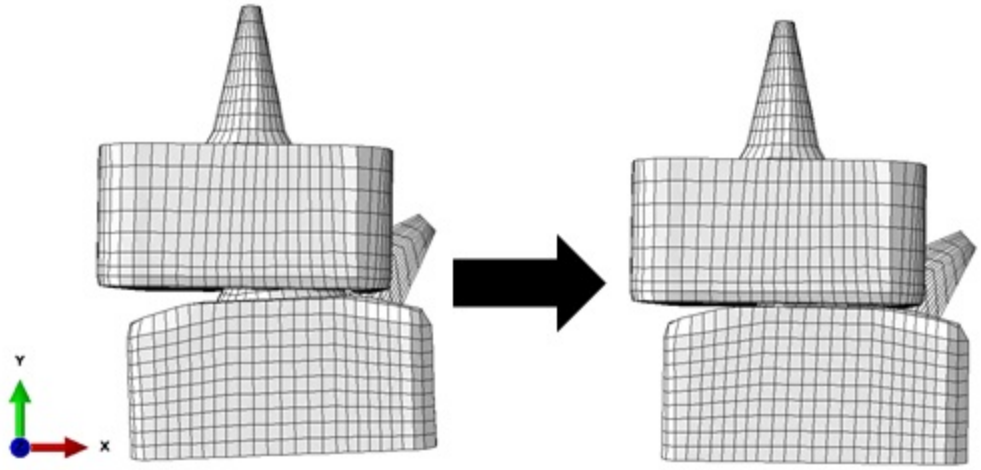

Figure 41: Displacement of the superior component relative to the inferior component.

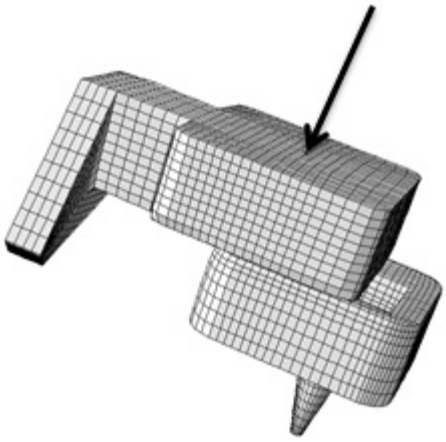

Figure 42: Compressive load applied to the posterior side of the superior component.

3.3.1.2 Results

After loading the backside of the superior component, the contact stresses on the inferior component surface were evaluated. Peak contact forces were located on the flat part of the inferior components (Figure 43). No forces were discovered in the "trough" section of the implant. The intent behind the design was to have stresses transfer from the superior articulating surface to the "trough" feature of the inferior component.

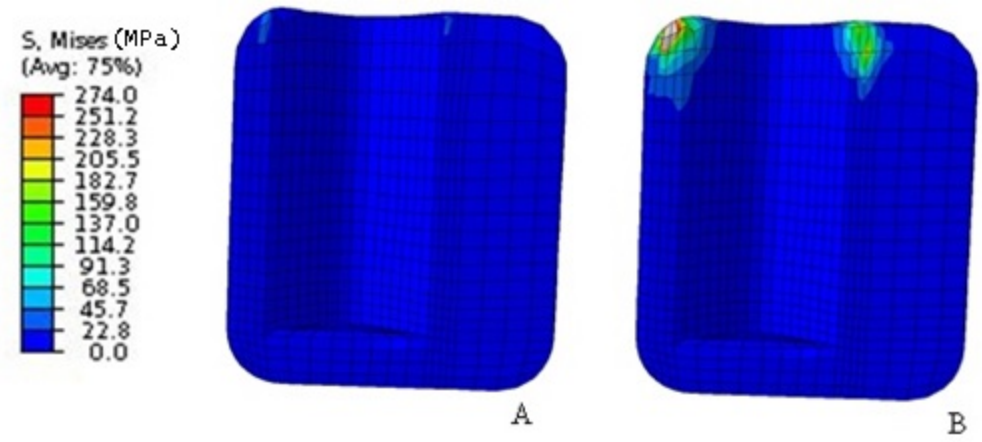

Figure 43: Contact stress results for metal-on-poly design (A) and metal-on-metal design (B).

The same compressive test that was constructed for the previous design was used for the third iteration. The contact stresses for the third design are concentrated in the "trough" of the inferior component, which agrees with the original design intent. The stresses (von Mises) for the metal-on-metal design are also much lower for Design III with a 274 MPa stress compared to the design II iteration with a 931.8 MPa stress. The stress on the poly design was higher than design II iteration but the stresses are located in the "trough" section of the inferior component which follows the design intent. Figure 44 represents the stress results on the inferior component for Design Iteration III.

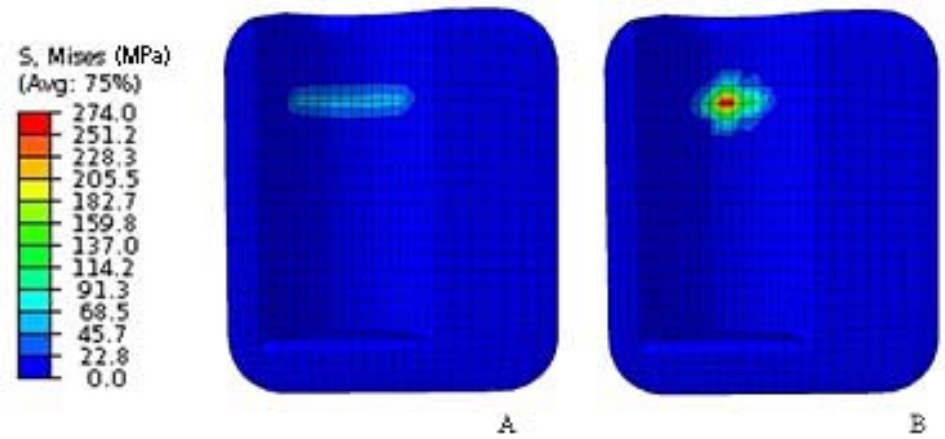

Figure 44: Third design iteration contact stress results for metal-on-poly design (A) and metal-on-metal design (B).

3.3.2 Anatomical Loading Test

3.3.2.1 Methods

After evaluation of the compressive model results, the left inferior and superior components of the third design were meshed. The components were modeled with 4,176 elements and 3,134 elements for the left inferior and left superior components, respectively. Both sets (right and left) were translated and rotated to the approximate location of the L4-L5 facets in ParaView (Version 3.6.1) shown in Figure 45.

Titanium was used for the study due to the excellent wear properties of the material. Contact surfaces were defined for the left implants similar to the compressive test. Similar to the compression test, the inferior side of the inferior components was held rigid. A reference node was assigned to the approximate location of the center of the L4-L5 disc.

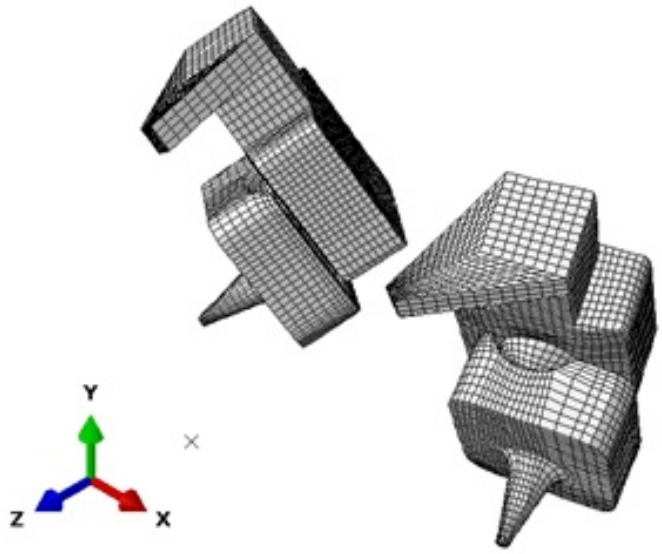

Figure 45: Anatomic position of the right and left implants at approximately the L4-L5 FSU.

The implants were first displaced and rotated to come into contact with the inferior components. The superior components were compressed to simulate the weight of the body superior to the lumbar region, 400 N. The implants were rotated in the following step while still loading the reference node. The final step was to release boundary conditions to allow the superior component to settle while the load was still being applied.

Prescribed rotations of the implants are shown in Table 1. Values used were results from previous studies reported in literature by Goel et al. [36], Rohlmann et al. [43] and Grosland [44]. The von Mises stresses were further evaluated.

Table 1: Rotations applied to the third design iteration.

Flexion	5.40°
Extension	3.40°
Left Lateral Bending	2.00°
Right Lateral Bending	1.70°
Left Axial Rotation	1.80°
Right Axial Rotation	1.90°

3.3.2.2 Results

The first set of implants to be examined was the flexion model (Figure 46A). These results were directly compared to the stresses developed for the extension model (Figure 46B). Stresses were more built up on the edges where the flat part and the curved part of the implants meet for both flexion and extension. Stresses were also found to be much higher for the flexion case compared to extension.

In addition to flexion/extension, lateral bending was also investigated. Figure 47 shows RLB (A) and LLB (B) on the same scale. Similar to flexion/extension, peak stresses were found on the edges of the implant as opposed to the "trough". The implants were also axially rotated; however the model was not able to run to completion. Reasons for this are discussed further in part 3.3.

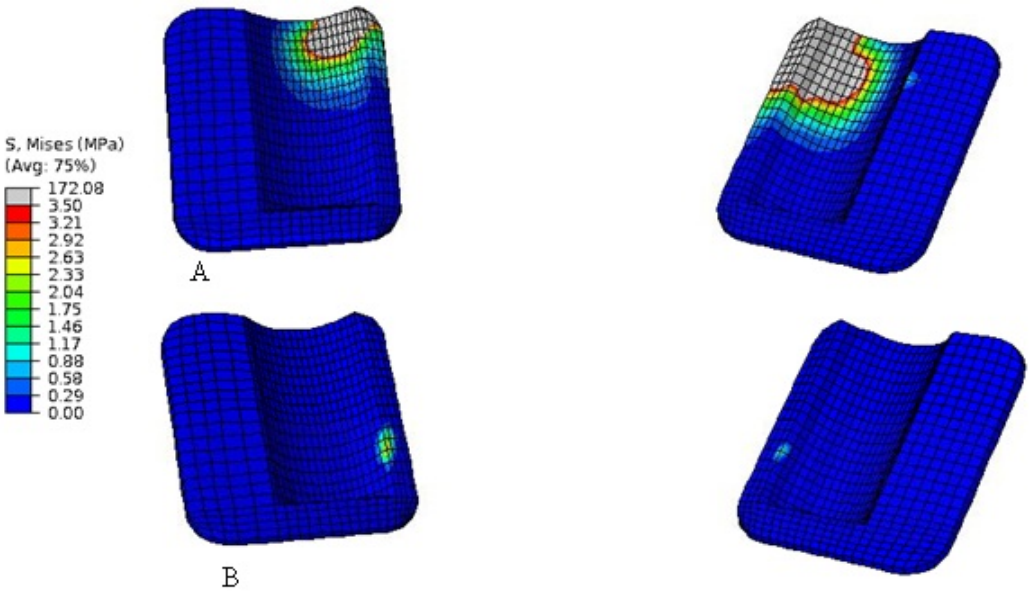

Figure 46: Flexion (A) and extension (B) von Mises results for Design Iteration III.

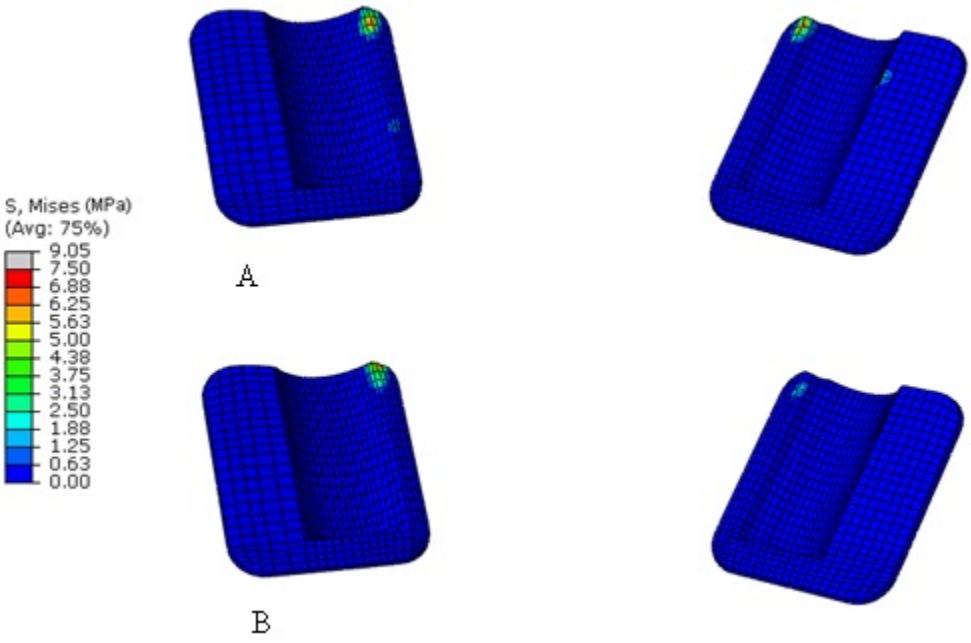

Figure 47: Direct comparison of von Mises stresses for RLB (A) and LLB (B) of Design Iteration III implants.

3.4 Discussion

The first iteration of the implant was discarded early in the design process. This was due to the non-conforming nature of the articulating surface. Large forces can be transferred through the facets in the lumbar spine and the geometry of the design implied the peg would break off and cause implant failure.

The second iteration of the design was created to be more conforming and to avoid failure from high forces. For comparison purposes, a third iteration was developed. The second design iteration was edited to create the third iteration. The "ball" and "trough" were redesigned to be more conforming than the previous version and more spherical in shape. This allowed for more contact between the two surfaces. What was once a flat surface on the superior component became angled to allow for more rocking motion when the superior and inferior components came into contact.

The first FE study was designed to compare Design Iterations II and III to determine which one to go forward with. Compressive loads led to contact forces on the flat portion of Design Iteration II. The dimensions of the design led to an implant that would contact the flat portion of the implants but the "ball" on the superior component was never able to reach the "trough" of the inferior component through unidirectional compression. Although this may not lead to any failure, the objective was to follow a design similar to hip implants where the acetabular cup and femoral head conform and stresses transfer so there is no peak stress on a small portion of the implant.

The third design was tested under the same conditions as the second design. Transference of the stresses took place in the "trough" of the inferior component leading to less of a point stress compared to the previous version. The implant will be less likely to deform due to the broader load to surface area ratio.

After compression testing, the third design was determined to be the design to move forward with. Another test was designed to evaluate performance under anatomical loading conditions. As the test progressed, it was determined that artificial

boundary conditions would need to be used in order to complete the analysis. Most degrees of freedom had to be held rigid while loads were applied. This leads to the question of whether these results foreshadow the results after the implant is introduced to the spine.

F/E and LB showed that stresses at the end of the test were transferred along edges of the "trough" and the flat portions of the implants. High contact forces may lead to deformations of the implants and eventual failure. Axial rotation was unable to run to completion. This is believed to be due to the lack of bony and soft tissue constraints that are present in the spine that help limit rotations. As these other factors are introduced, axial rotation of the implant will be able to run to completion and the other motions will present with better results of location of stresses.

CHAPTER 4

LUMBAR FE MODEL DEVELOPMENT AND VALIDATION

4.1 Introduction

A finite element model of the lumbar spine (L3-L5) was created to study the effects of the facet replacement and other surgical procedures. An intact model was developed from an image dataset and validated with literature results. After validation of the intact model, two decompression lumbar surgeries and a model with artificial facets at the L4-L5 were simulated. The biomechanical effects of the different procedures were compared to the intact model, focusing on the changes in ROM, facet contact forces and IVD stresses.

4.2 Materials and Methods

4.2.1 Intact Model

4.2.1.1 Vertebral Body Pre-Processing Techniques

CT data was acquired from a cadaveric specimen (48 year old male) at 1 mm slices. To create surfaces from the image, data was imported into BRAINS2 software [45, 46]. The L3, L4 and L5 vertebra were segmented and STL surfaces were created using Gaussian image-based smoothing techniques. The segmentation technique used was similar to the process described by DeVries et al. [47].

To simplify the meshing of the complex geometry of the vertebra, each surface was separated into two regions, the vertebral body and posterior region, and meshed separately. The body was clipped from the posterior complex using in-house software [48]. A plane clip and the box clip function were used to clip the posterior region from the body at the pedicles to be as close to the body as possible (Figure 48).

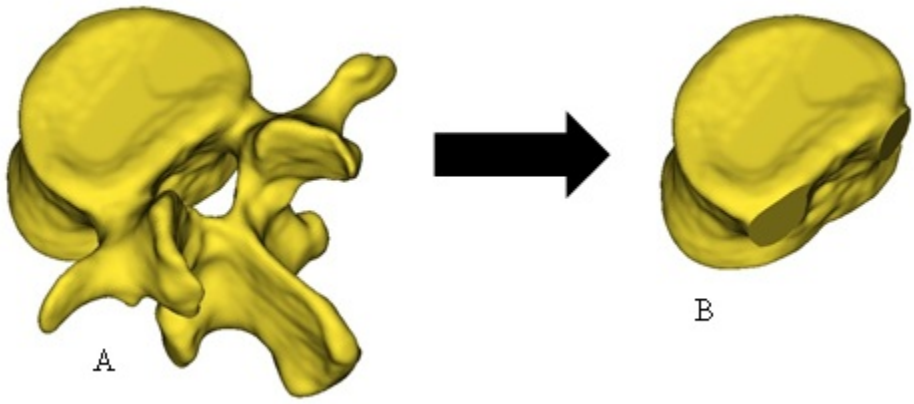

Figure 48: The L3 vertebra surface before clipping (A) and after clipping (B).

IA-FEMesh, was used for mesh generation of the vertebral body [40]. A butterfly block technique was used to create a hexahedral mesh of the body. This technique is explained in detail by Kallemeyn et al. [49]. Feature edges of the outer edge and the perimeter of the nucleus pulposus were constructed to help capture the regions of the vertebral body. The purpose of this technique was to simulate the lamellae of the annulus fibrosus and the nucleus pulposus of the discs. The feature edges were defined such that the nucleus accounted for approximately 44% of the disc area and the nucleus was centered 3.5 mm posterior to the center of the body [50].

A mesh seeding was initially chosen as 15 elements along the poster/anterior direction, 21 elements length along the cranial/caudal direction, 3 elements length in the radial 1 direction and 4 elements in the radial 2 direction (Figure 49). After application of the seeding, a mesh was created shown in Figure 50.

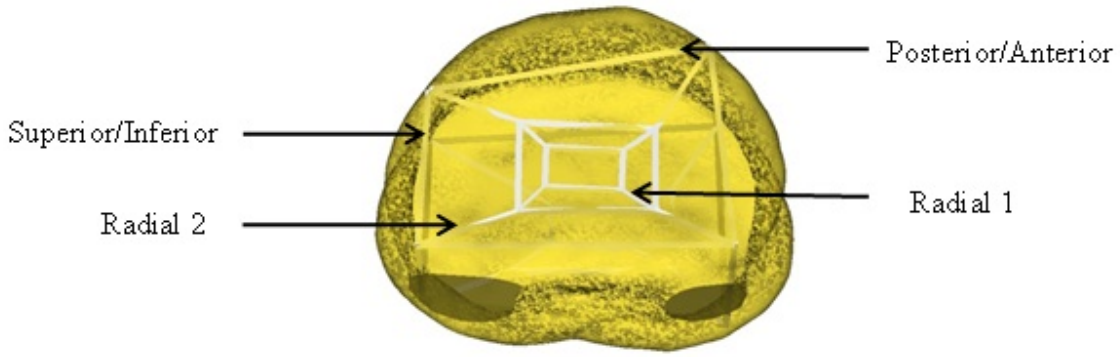

Figure 49: Butterfly building blocks of the L3 vertebral body.

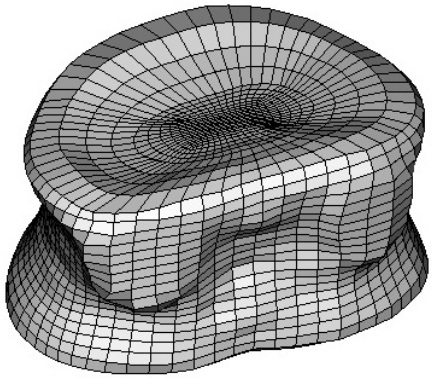

Figure 50: A complete mesh of the L3 vertebral body.

4.2.1.2 Convergence Study

To determine an optimal number of elements, a convergence study was conducted on the L3 vertebral body. With the initial mesh seeding, the body consisted of 14,805 elements. The outer most elements were assigned cortical material properties and the inner elements were defined as cancellous [51].

A previous convergence study performed by Rohlmann et al.[43] loaded the superior body to 500 N while the inferior nodes were held rigid. Resultant stresses of three nodes were evaluated after application of the load. Locations were chosen in

regions where there would be no artificially high stresses due to the load. The locations of these nodes are shown in Figure 51. The mesh seeding ratio was kept approximately the same for each compression test. Additional meshes created for the test consisted of 2,925 elements, 5,775 elements, 24,225 elements, 30,267 elements and 47,740 elements.

Results for Node 3 are shown in Figure 52; the other figures for Node 1 and Node 2 are located in Appendix A. The Node 2 results show that as the number of elements increased there was approximately a positive linear trend with respect to the stress. However, the stress at 30,267 elements dropped drastically and then increased again. There was no point in which the stresses leveled off so this information was not used to determine mesh seeding.

The stresses at Node 1 began to asymptote at 24,225 elements, but rose at 47,740 elements. Node 3 stresses began to level off at 14,850 elements and rose at 47,740 elements, similar to the Node 1. The mesh seeding that produced 14,850 elements was chosen over the seeding that produced 24,255 elements due to the importance of the posterior region over the vertebral body/intervertebral disc. Meshes for L4 and L5 vertebral bodies were created using the same techniques and mesh seeding used for L3.

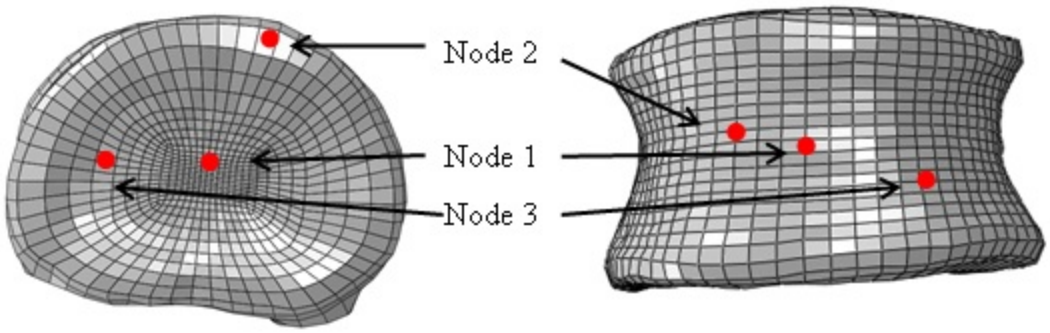

Figure 51: Defined node locations to evaluate stresses during the convergence test.

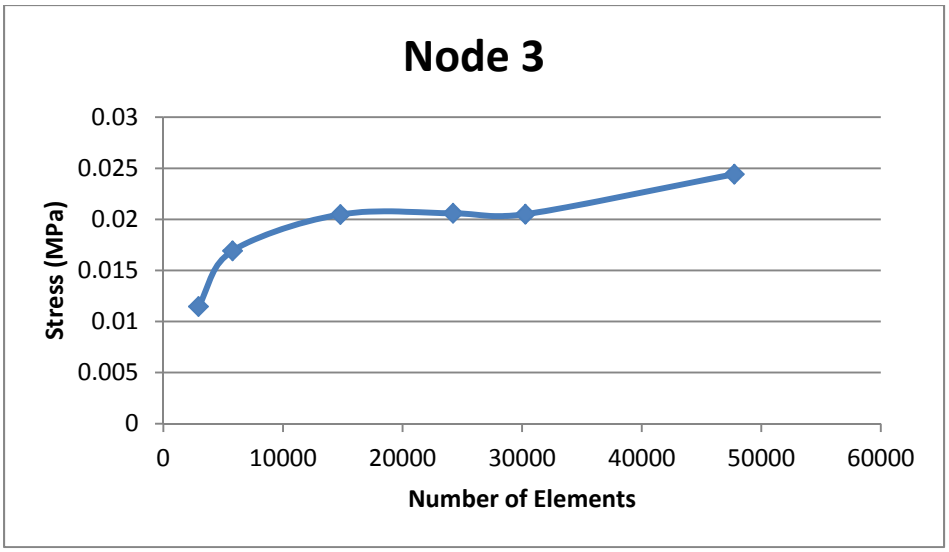

Figure 52: Results of convergence test performed on the L3 vertebra.

4.2.1.3 Other Pre-Processing Techniques

After a convergence study was performed, the posterior region of the L3 vertebra was developed. Blocks were initiated at the pedicle region with vertices being "snapped" to nodes of the L3 vertebral body at the perimeter of the pedicles. Feature edges were created at the region where the pedicle was cut to allow the meshes to integrate properly and to better capture the pedicles. The blocks propagated posteriorly from each side of the posterior region and merged at the lamina, near the spinous process. A complete multi-block formation of the posterior region is shown in Figure 53. The meshes were more refined at the facets, since this was a region of interest. Other regions were coarser due to the secondary importance of these regions. A figure of the L3 vertebra after mesh refinement is shown in Figure 54.

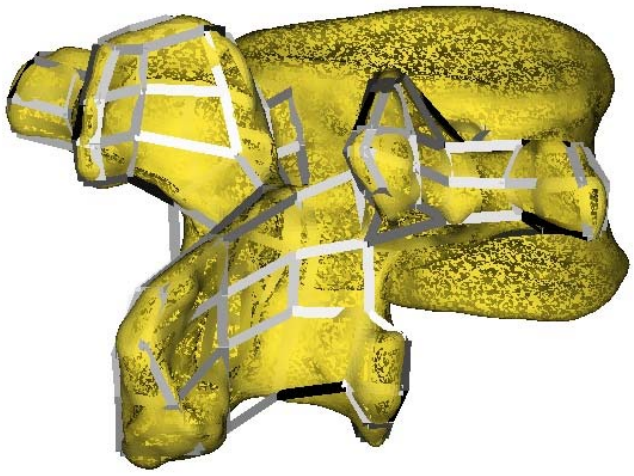

Figure 53: Multi-block technique of the posterior region.

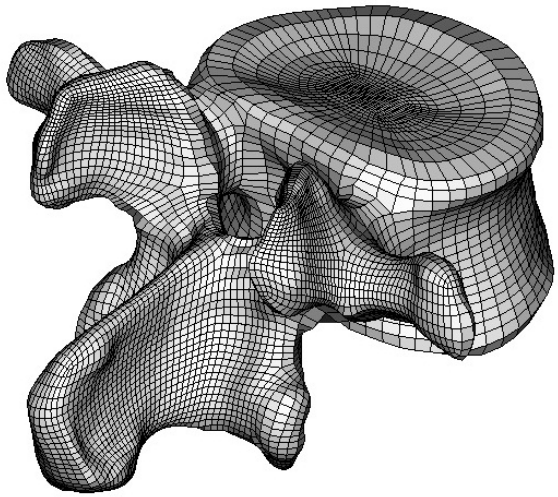

Figure 54: Refined mesh of the L3 vertebra.

A building block mapping algorithm previously developed in-house was used to create the building blocks for the L4 and L5 posterior vertebral region [52, 53]. The intervertebral discs were interpolated between the respective vertebrae with a height of eight elements. This allowed for continuity between the discs and the vertebra. The

ligaments attachment sites were defined based on approximate locations reported by Cramer and Darby [5].

4.2.1.4 Material Properties

Material properties were gathered from relevant literature and were assigned to the L3-L5 model (Table 2). Similar to the convergence test, the outer elements of the vertebral body were assigned as cortical bone and the inner elements as cancellous bone [51]. The posterior bone was assigned separate material properties from the body [51].

The intervertebral discs were modeled as four annulus layers surrounding the nucleus pulposus. Each annulus was imbedded with four layers of crisscrossing hypoelastic fibers at ±30° to the transverse plane [54, 55]. The ground substance was defined with the Mooney-Rivlin law. Values of 0.56 and 0.14 were assigned to c_1 and c_2 [50]. The nucleus pulposus was modeled as an incompressible fluid [43]. The volume of fibers in the annulus fiber was 16% of the annulus fibrosus [56].

Seven ligaments were defined in the lumbar modeled. These include the ALL, PLL, LF, ISL, SSL, ITL and CAP. The ligaments were modeled as nonlinear 3D truss elements. Values for cross-sectional area and modulus of elasticity are listed in Table 2.

Facet cartilage was modeled as a tabular-pressure-overclosure relationship. An initial minimum distance between the bony surfaces was determined prior to the addition of loads or moments. From these values, a cartilage thickness was calculated at a contact pressure of 0 MPa. The pressure increases as the distance between the two surfaces decreases. The L3-L5 intact model is shown in Figure 55.

Table 2: Mechanical characteristics of the intact lumbar spine

Component	Element Type	Modulus of Elasticity (MPa)	Poisson's Ratio	Cross-sectional Area (mm^2)
Vertebral Body [51]				
Cortical Bone	C3D8	12,000	0.3	
Cancellous Bone	C3D8	100	0.2	
Posterior Bone [51]	C3D8	3,500	0.25	
Intervertebral Disc				
Nucleus Pulposus [43]	F3D4	1	0.499	
Ground Substance [50]	C3D8H	≈4.2	0.45	
Annulus Fibrosus [54]	Rebar		0.3	
Ligaments [6]				
ALL	T3D2	7.8 (<12%), 20.0 (>12%)	0.3	74
PLL	T3D2	10.0 (<11%), 20.0 (>11%)	0.3	14.4
LF	T3D2	15.0 (<6.2%), 19.5 (>6.2%)	0.3	40
ISL	T3D2	10.0 (<14%), 11.6 (>14%)	0.3	40
SSL	T3D2	8.0 (<20%), 15.0 (>20%)	0.3	30
ITL	T3D2	10.0 (<14%), 11.6 (>14%)	0.3	1.8
CAP	T3D2	7.5 (<25%), 32.9 (>25%)	0.3	34

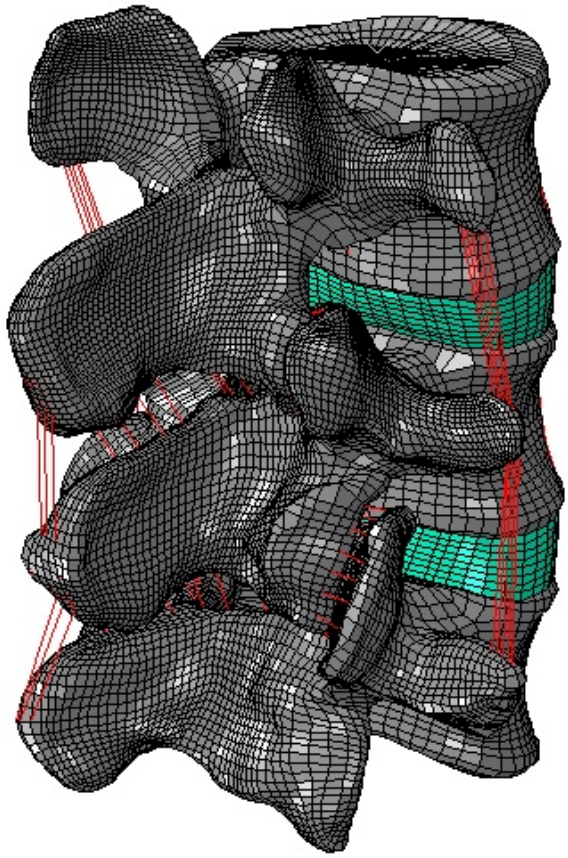

Figure 55: A complete L3-L5 model.

4.2.1.5 Boundary and Loading Conditions

The most inferior nodes of the L5 were fixed in all directions. A rigid surface was created on the superior side of the L3. All moments and loads were applied to this surface. A preload of 400N was applied, followed by the loading moment [44]. The moment applied was ±10 Nm for flexion/extension, lateral bending and axial rotation [57].

4.2.2 Laminectomy and Facetectomy Models

To further compare the effect of the facet implant, a laminectomy model was created. The spinous process and part of the lamina was removed at the L4-L5 (Figure

56). The CAP, ITL, PLL and ALL were preserved. The boundary and loading conditions were the same as the intact model.

Furthermore, the contact definitions at the L4-L5 were removed from the intact model for a 100% bilateral facetectomy. The contact at the L3-L4 remained intact. As stated by Natarajan et al., the capsular, ligamentum flavum and the interspinous ligament were resected during a complete bilateral facetectomy procedure [8]. Boundary and loading conditions were the same as intact.

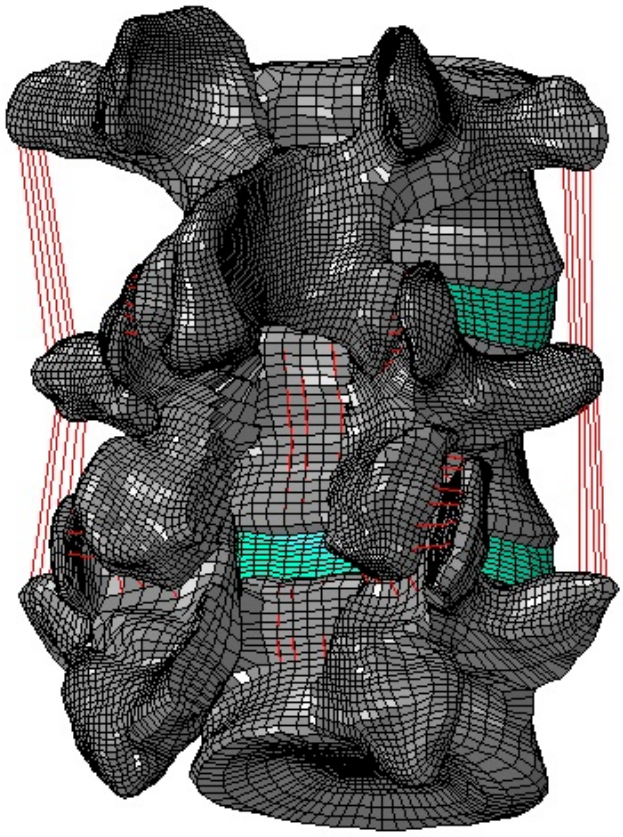

Figure 56: A L4-L5 laminectomy model.

4.2.3 Implanted Spine Model

Before implanting the devices, elements that compose the L5 superior facets, L4 inferior facets and part of the pedicles were removed from the intact model. The L4-L5 capsular ligament and the ligamentum flavum were removed to simulate a surgical procedure. The L3-L4 facet contact remained intact.

The attachment sites of the components were fixated to the pedicles of the respective vertebra. The implants were modeled as titanium implants (E=100 GPa, v=0.32). The finite-sliding surface interaction was modeled with a coefficient of friction of 0.3. Figure 57 shows the implants after insertion into the spine.

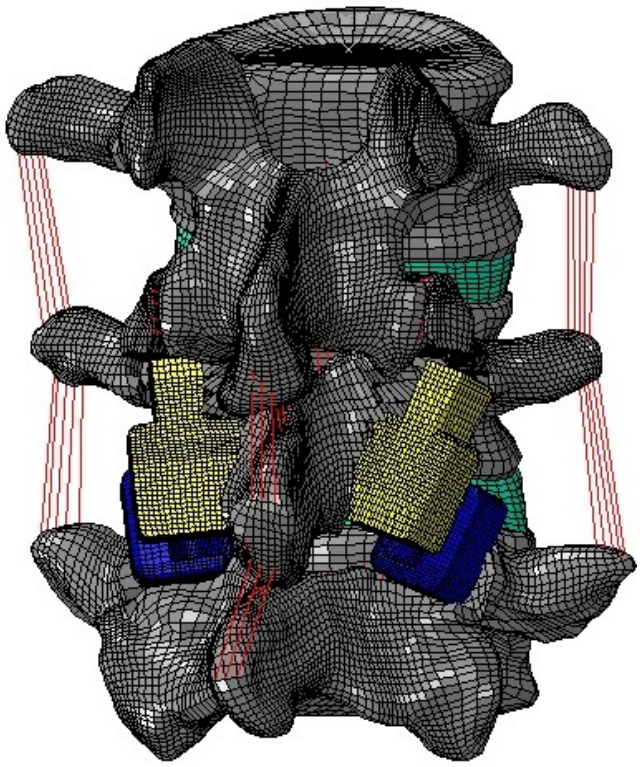

Figure 57: L3-L5 model with an L4-L5 facet replacement.

Boundary conditions were the same as the intact model but loading conditions were edited. After displacing the superior component into contact, the same preload applied to the intact and degenerated models was applied. Instead of applying a moment of ±10 Nm, rotations amounts that resulted in approximately a ±10 Nm moment about the rigid surface were applied.

4.3 Results

4.3.1 Kinematics

The ROM was calculated and compared for all the models. The intact model motion is displayed in Figure 58 and raw values are shown in Table B-1 and Table B-2. The motion at each FSU was validated against literature results (Table 3 and Table 4).

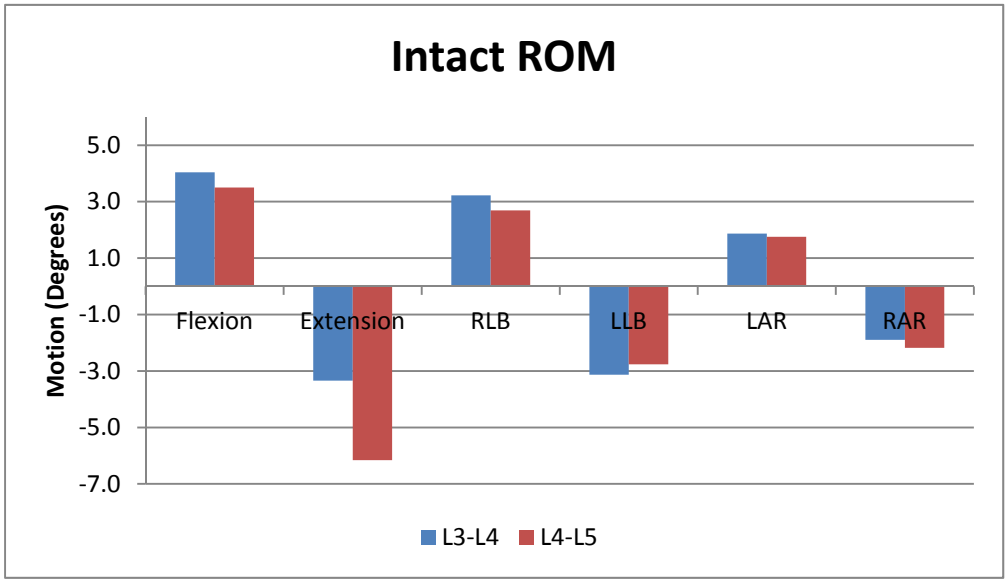

Figure 58: Intact ROM for both L3-L4 and L4-L5.

Table 3: Literature results of ROM at the L3-L4 FSU.

Group	Flexion (°)	Extension (°)	LB (°)	AR (°)
Goel [6]	FE: 5.034 Exp: 4.235 ± 1.765	FE: -3.655 Exp: -2.667 ± 0.902	N/A	N/A
Kiapour [58]	FE: 5.00	FE: -2.40	FE: 4.70	FE: 2.60
Rohlmann [57]	FE:6.05	FE: -3.277	FE: 5.092	FE: 2.269
Chen [59]	FE: 3.96	FE: -3.644	FE: 4.238	FE: 2.455
Chen [60]	FE: 3.58	FE: -1.18	FE: 3.33	FE: 2.21
Grosland [44]	FE:5.324 Exp: 5.51 ± 1.00	FE:-3.445 Exp: -2.99 ± 1.02	FE: 5.134 R. Exp: 5.64 ± 1.22 L. Exp: 4.90 ± 0.79	FE:2.978 Exp: 1.50 ± 0.67

Table 4: Literature results of ROM at the L4-L5 FSU

Group	Flexion (°)	Extension (°)	LB (°)	AR (°)
Goel [6]	FE: 4.828 Exp: 5.020 ± 2.824	FE: -3.517 Exp: -4.00 ± 0.980	N/A	N/A
Goel [36]	FE: 4.483 Exp: 6.138 ± 2.155	FE: -3.345 Exp: -3.241 ± 1.69	FE: 4.517 Exp: 4.276± 1.655	FE: 2.724 Exp: 2.310 ± 0.914
Dooris [61]	FE: 5.88	FE: -3.70	N/A	N/A
Kiapou [58]	FE: 5.00	FE: -2.70	FE: 4.50	FE: 2.40
Rohlmann [43]	Exp: 7.135 ± 2.331	Exp: -4.888 ± 0.955	Exp: 3.458 ± 1. 354	Exp: 3.417 ± 1.354
Chen [59]	FE: 5.20	FE: -4.343	FE: 4.914	FE: 2.829
Chen [60]	FE: 4.49	FE: -3.89	FE: 2.08	FE: 2.08
Grosland [44]	FE:5.081 Exp: 5.51 ± 1.00	FE:-3.351 Exp: -2.99 ± 1.02	FE:5.181 R. Exp: 5.64 ± 1.22 L. Exp: 4.90 ± 0.79	FE:2.75 Exp: 1.50 ± 0.67

After validation of the motion for the intact case, the motions of the various surgical procedures were compared. After a laminectomy was simulated at the L4-L5 FSU, the L3-L4 level motion increased for flexion and LAR by 38.27% and 5.81%, respectively. Other motions only differed by less than 1.8% (Figure 59). At the L4-L5 level, flexion, LAR and RAR had changed more than 11% from intact. Flexion increased 79.25%, LAR increased by 23.63% and RAR increased from intact by 11.47% (Figure 60).

The 100% bilateral facetectomy model had little changes from the intact model at the L3-L4 level (Figure 59). Flexion showed the largest change with only a 5.59% increase. The L4-L5 level, however, showed large changes. The largest change was in AR with an increase of 193.05% for LAR and 126.78% for RAR. Flexion/extension increased 88.55% for flexion and 20.34% for extension, relative to intact (Figure 60).

After the simulation of surgical treatments, the implants were fixated to the approximate location of the L4-L5 facets after facet removal. Shown in Figure 59, motion agreed with intact at the L3-L4 level after insertion of the components. At the L4-L5 level, motion did not differ for RLB and LAR. RAR was 26.62% less than intact RAR. LLB and flexion was 16.04% less and 20.27% more than intact motion, respectively. Extension motion decreased the most compared to the other motions at this level with 63.82% decrease from intact extension (Figure 60). Raw values of ROM at the L3-L4 and L4-L5 level are shown in Appendix B, Table B-1 and Table B-2, respectively.

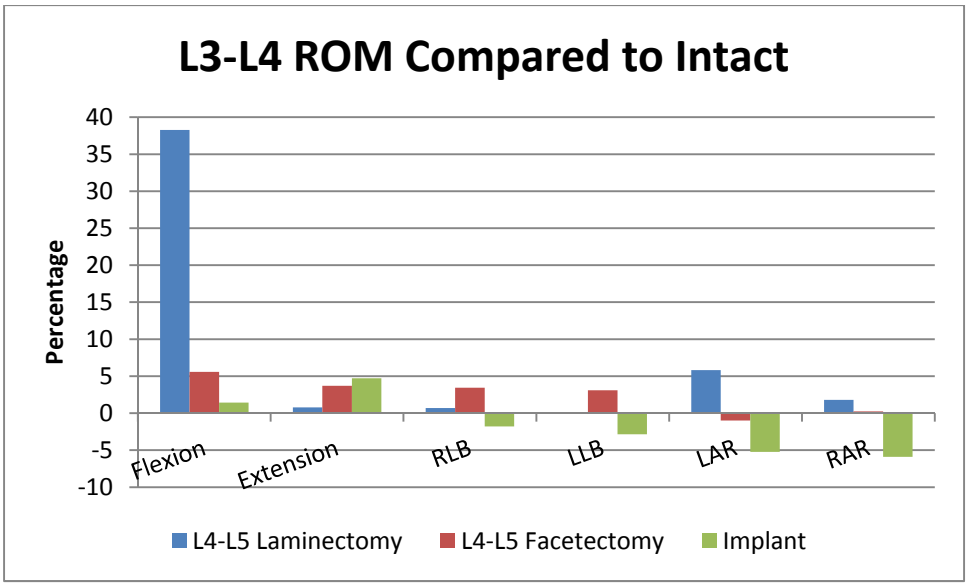

Figure 59: Surgical treatments' ROM represented as a percentage of the intact motion at the L3-L4 level.

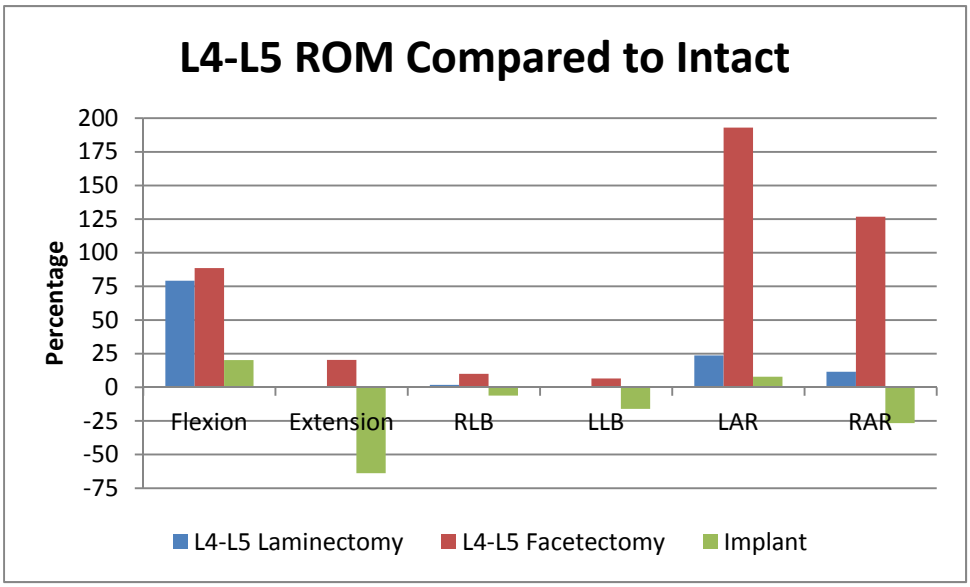

Figure 60: Surgical treatemtents' ROM represented as a percentage of the intact motion at the L4-L5 level.

4.3.2 Facet Contact Forces

Another aspect of the model that was validated was the contact forces at the L3-L4 and L4-L5 facets (Table 5 and Table 6). The intact facet forces are shown in Figure 61 and raw values are in Appendix B, Tables B-3, B-4, B-5 and B-6.

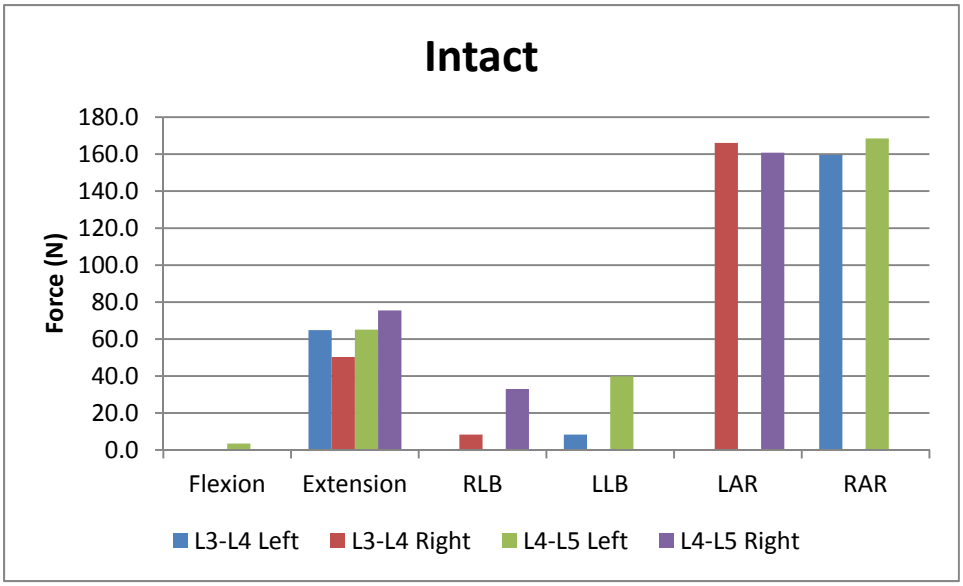

Figure 61: Facet contact forces for the intact case.

Table 5: Literature facet contact forces at the L3-L4 FSU

Group	Extension (N)	Lateral Bending (N)	Axial Rotation (N)
Dooris [61]	166.00	N/A	N/A
Goel [6]	318.60	N/A	N/A
Rohlmann [50]	319.00	359.00	174.00
Rohlmann [57]	30.15	5.54	119.39
Schmidt [62]	31.69	N/A	N/A
Chen [60]	161.00	N/A	N/A
Kuo [29]	Rt: 213.21 Left: 128.93	N/A	Rt, RAR: 92.98 Left, RAR: 119.88 Rt, LAR: 199.42 Left, LAR: 114.53
Sawa [32]	319.00	N/A	N/A
Kiapour [58]	171.80	Rt: 54.10 Rt: 8.90	161.00

Table 6: Literature facet contact forces at the L4-L5 level

Group	Extension (N)	Lateral Bending (N)	Axial Rotation (N)
Goel [6]	625.60	N/A	N/A
Goel [36]	163.00	64.00	151.00
Schmidt [62]	40.31	N/A	
Chen [60]	155.00	N/A	
Kuo [29]	Rt: 167.30 Left: 76.73	N/A	
Sawa [32]	326.00	N/A	Rt, RAR: 55.56 Left, RAR: 106.43 Rt, LAR: 169.19 Left, LAR: 130.23
Kiapour [58]	163.60	Rt: 13.10 Left: 58.80	159.60

On the left side of the L3-L4 (non-operated) level, the contact forces greatly increased when the implant was added. For extension, contact forces increased by

38.28% compared to intact. Facet forces increased 33.55% for LLB and 9.84% for RAR. Laminectomy had little effect on the L3-L4 level; the L4-L5 facetectomy increased L3-L4 facet force for LLB by 17.24% but the other two motions had little change.

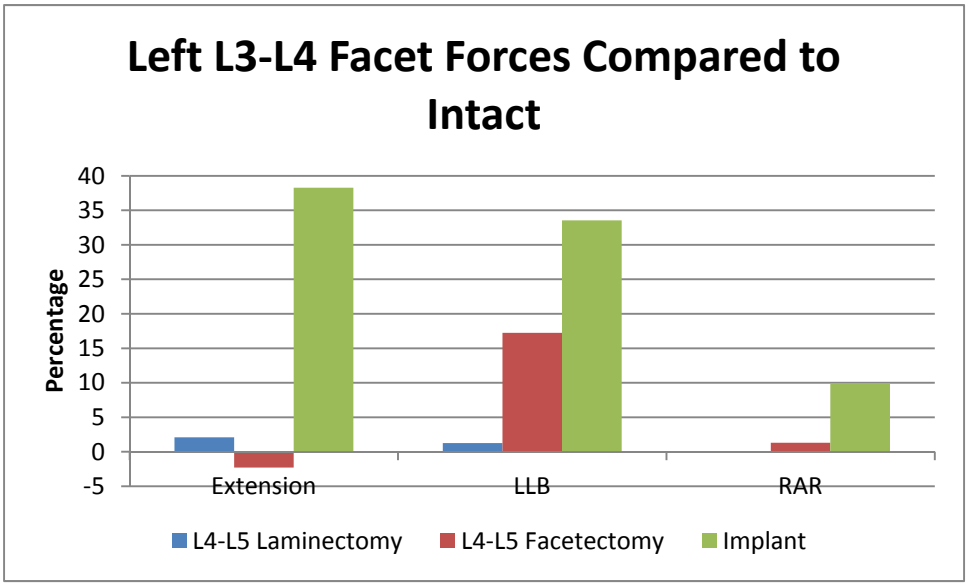

Figure 62: L3-L4 left facet results as a percent of intact for surgical treatment models

The L3-L4 right side facet force decreased extension by 26.91% and LAR decreased by 4.15% after facet implantation at the L4-L5. RLB contact forces increased by 53.18% from intact. Similar to the left side, a laminectomy had little effect on the forces at L3-L4 and L4-L5 facetectomy increased L3-L4 facet forces by 17.32% during RLB.

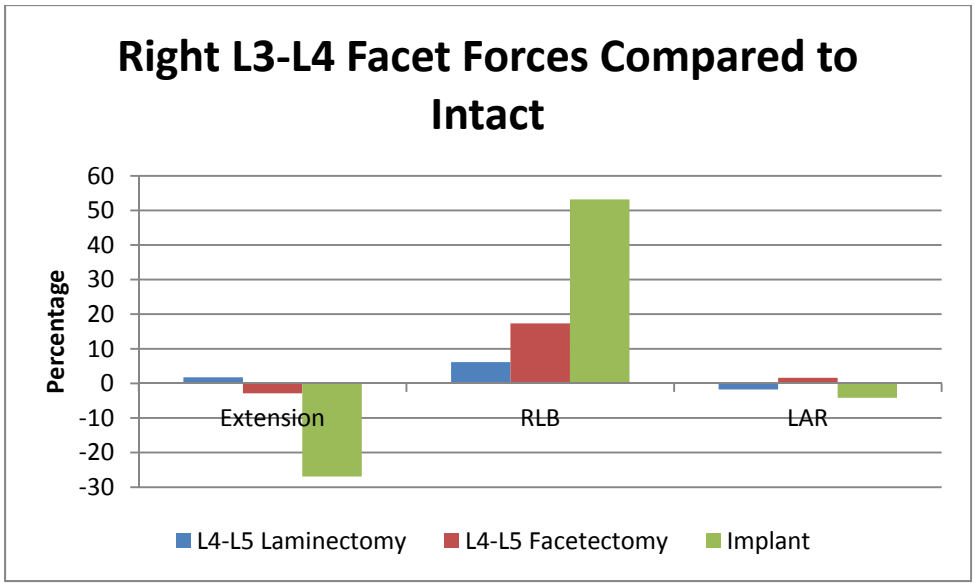

Figure 63: Comparison of the intact case at the L3-L4 left facet to the surgical treatments.

Contact forces on the left side of the L4-L5 (operated level) showed similar trends to those at the L3-L4 (non-operative level). However, the percent change after components were inserted from intact was much larger than the adjacent level (L3-L4) change. Extension contact forces increased by 213.76%, LLB increased by 125.77% and RAR increased by 18.40% (Figure 64). Laminectomy had minimal change on the facet force compared to intact; the largest change was a decrease in forces during RAR (9.20%).

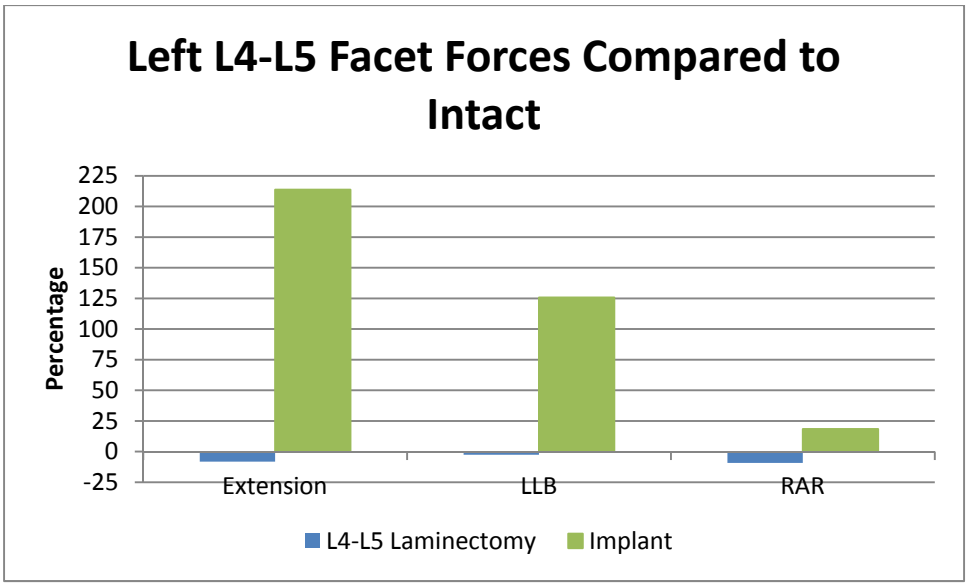

Figure 64: Comparison between all cases at the left L4-L5 facet represented as a percent of intact.

In addition to the left side, the right side of the L4-L5 level was evaluated and is shown in Figure 65. After the implant was added to this level, extension contact forces increased 233.64% from intact and RLB increased 146.99% from intact. LAR only increased 4.54% from intact. The laminectomy at the L4-L5 level showed little change from the intact state with extension decreased by 6.73%, RLB decreased by 7.54% and LAR decreased by 1.68%.

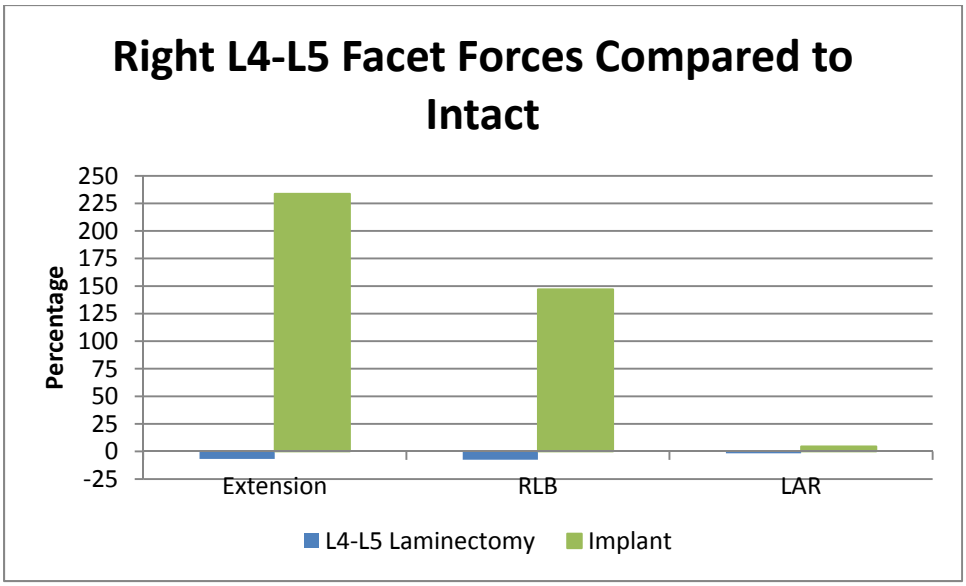

Figure 65: Comparison of the right facet contact forces at the L4-L5 level represented as a percent of intact.

4.3.3 Disc Stresses

In addition to ROM and facet contact force evaluation, the von Mises stresses in the discs were compared between the intact and the three surgical models. The stresses in each region were evaluated depending on the motion of the spine. Stresses were averaged for the anterior region for flexion, posterior region for extension, left lateral region for LAR and LLB and the right lateral region for RAR and RLB. The first graph is a representation of the stresses in the disc for the intact lumbar spine (Figure 66). Stresses in the L4-L5 IVD were higher than the stresses in the L3-L4 IVD.

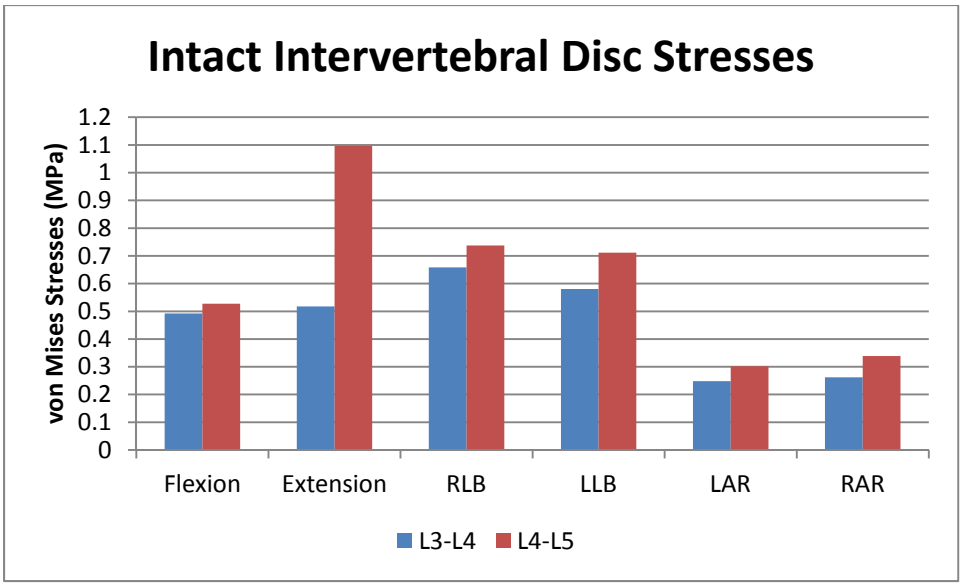

Figure 66: Intact IVD von Mises disc stresses

Von Mises stresses in the disc for the surgical treatments were compared to the intact case (Figure 67). At the L3-L4 level, stresses increased slightly in extension after the device was implanted at the L4-L5 level. The increase was 8.14% from intact. LAR stresses decreased by 7.05% from intact. All other stresses were less than 3.00% change from intact. An L4-L5 facetectomy changed the stresses very little with the largest change in flexion at 5.86% from intact. Laminectomy did not differ from the intact case except for the flexion test. In flexion, stresses increased by 29.98% from intact.

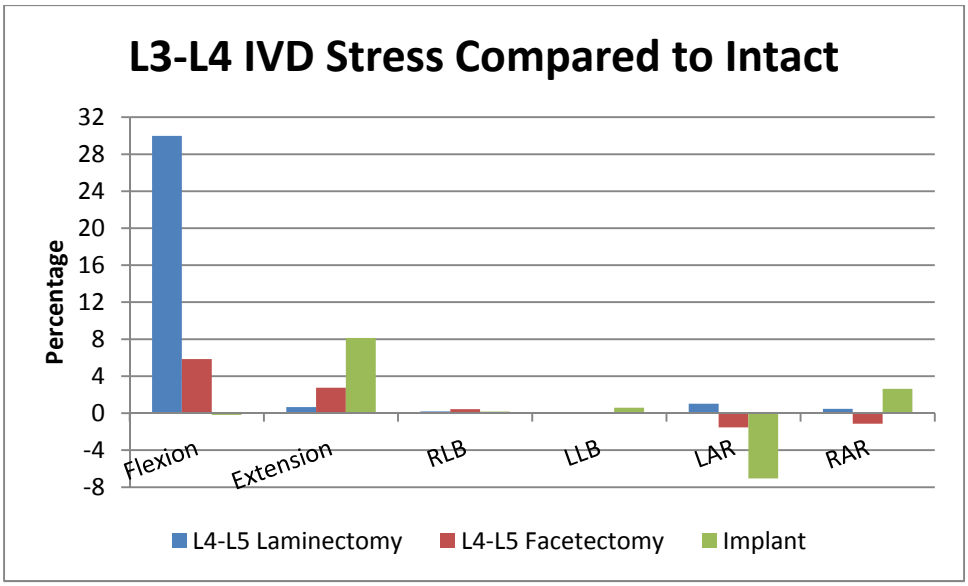

Figure 67: L3-L4 von Mises stress compared as a percent of intact stresses at the L3-L4.

Stresses in the operated level decreased when the implants were inserted for extension, lateral bending and RAR (Figure 68). During extension, stress decreased 66.22% from intact, 7.84% decrease from intact during RLB, a decrease of 9.38% in LLB and 3.25% decrease in RAR from intact. The other motions increased by 17.02% and 8.67% from intact for flexion and LAR, respectively.

For the decompressive surgeries, disc stresses increased for the flexion test at the operated level (Figure 68). Facetectomy increased 71.74% and laminectomy increased 65.14% from intact. The disc stress contours can be seen in Figure 69 and 70 for all four cases of extension and flexion, respectively.

Besides flexion, stresses for the laminectomy case did not change considerably from intact except for LAR. This motion increased stresses 12.12% from intact. A L4-L5 facetectomy caused an increase in disc stresses for all motions. Extension increased from intact by16.79% and LAR increased stresses by 64.84% from intact. RAR test caused stresses to increase by 32.07% and RLB and LLB increased stresses by less than

7.00% from intact. Raw values for all models are located in Appendix B, Table B-7 and Table B-8.

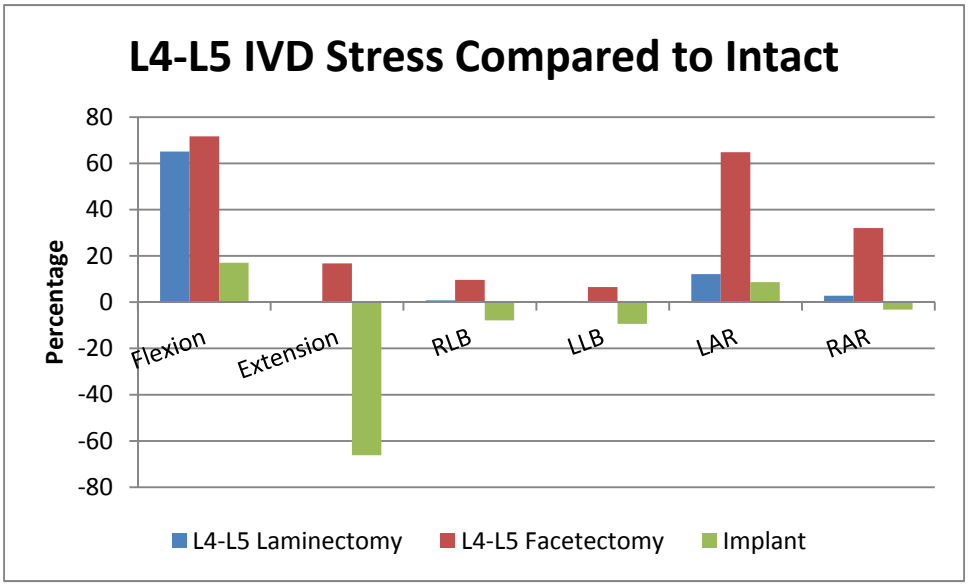

Figure 68: L4-L5 von Mises stresses compared as a percent of intact stresses at the L4-L5.

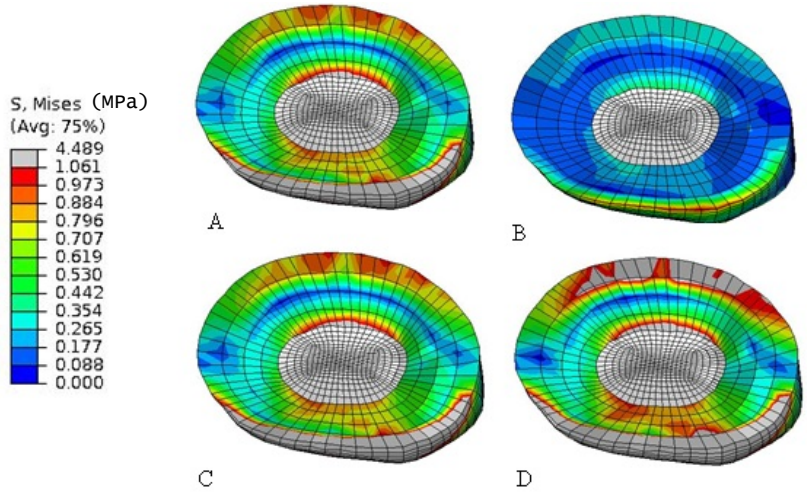

Figure 69: L4-L5 von Mises disc stresses after extension test for intact (A), implanted (B), laminectomy (C) and facetectomy (D).

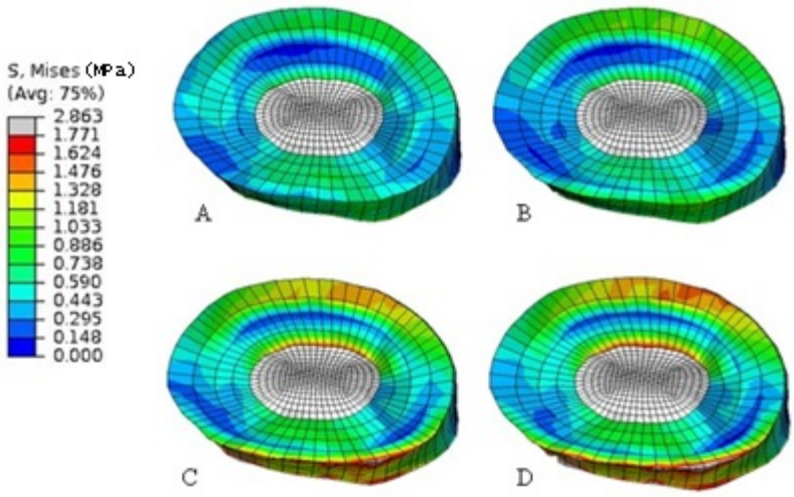

Figure 70: L4-L5 von Mises disc stresses after flexion test for intact (A), implanted (B), laminectomy (C), facetectomy (D).

4.4 Discussion

FE models were created of the L3-L5 spine to test the kinematics of the spine after insertion of the implant. Three different results were analyzed and compared to intact and two different surgical interventions that do not require implants.

The ROM of the intact model was validated with the literature results. All motion results were within the range of the given literature values (Table 3 and 4) except for LB at the L3-L4 level and L4-L5 extension. However, these values were near the literature values reported. RLB at the L3-L4 level had an error of 0.105° and LLB had an error of 0.201° from literature values. Extension at the L4-L5 level had an error of 0.316° compared to the literature values. Since the primary motion at the lumbar level is flexion/extension the LB discrepancies at the L3-L4 level were not a concern for further results of contact forces and disc stresses [5].

An objective of the design was to produce kinematics in the spine that were similar to intact levels after insertion of a facet replacement device. At the non-operated level (L3-L4), motion was restored in flexion/extension and LB to near intact levels. Flexion/extension was 2.91% larger than flexion/extension for intact case. Compared to

the decompression surgeries that were simulated, motion was 4.74% larger than intact for a L4-L5 facetectomy and 21.29% larger than intact for a L4-L5 laminectomy. Lateral bending for the implant model was 2.31% less than intact lateral bending. A laminectomy produced a LB motion that was 0.38% greater than intact and a facetectomy procedure was 3.27% larger than intact. Axial rotation was restricted by 5.53% of intact rotation while laminectomy increased motion by 3.38% of intact and facetectomy decreased by 0.34% of intact motion. The implant improved flexion/extension motion at the adjacent level compared to a laminectomy and a facetectomy, however a laminectomy was better at returning lateral bending to intact levels and a facetectomy returned rotation to near intact better than the implanted device.

At the surgical level, flexion was restored to intact but extension was restricted to 3.93° less than intact. When the implant was inserted at this level, lateral bending (both right and left) was evaluated to have decreased from intact lateral bending motion by 11.15%. Axial rotation after the device was inserted was 2.18° less than intact rotation. Decompression surgery resulted in increased flexion/extension motion compared to intact with 28.95% of intact flexion/extension for a laminectomy and 45.07% of intact for the same motion. Similar to the L3-L4 level, a laminectomy procedure did not considerably alter from intact motion with an increase in bending motion 0.94%. A facetectomy increased motion to 8.24% of intact. When axial rotation was tested with each of the decompression surgeries, a laminectomy increased motion to 16.91% of intact motion and a facetectomy surgery increased motion by 156.34% of intact motion.

A laminectomy was able to restore most motion but increased considerably from intact when the spine experienced flexion. Facetectomy captured intact level secondary motions (LB and AR) at the L3-L4 but other motions at the operated level and flexion/extension at the adjacent level were considerably different than intact motion. The implant was better able to restore motion to near intact levels for both FSUs for all motions compared to a decompression surgery.

Similar to the ROM, contact forces were validated for the intact case against literature results in Tables 5 and 6. Flexion produced a facet force of greater than 0 N on the left side of the facet joint for both levels. However, since the contact forces for all other motions were validated with literature values this was not considered as a concern for validation purposes.

During the flexion test, the device caused an increase in contact forces on both facets at each level. This was also a trend for the left L3-L4 extension, L3-L4 lateral bending and RAR. The right facet joint of the L3-L4 FSU experienced a decrease in contact forces during extension and LAR. Contact forces at the L4-L5 level are considerably higher than intact for all motions.

The discrepancy between the two joints at the non-operated level highlights the issue of uneven placement of the implants at the L4-L5 level. No instrumentation or morphological markers were used when the implants were inserted. This was most noticeable when the spine was extended. As the spine began extending, one superior implant would hit the corresponding inferior implant first before the other side.

Another issue is adjacent level degeneration. Contact forces were as much as 53.18% larger (RLB) than the intact motion and left facet extension resulted in a 24.8 N larger contact force than intact results. The disagreement of forces between intact and the implanted spine may lead to degeneration at the healthy, non-operated level.

A final resultant that was further investigated was the von Mises stresses in the intervertebral disc. The implant disc stresses were near intact levels at the L3-L4 FSU for all motions. At the L4-L5 level, AR and LB was close to intact stress levels but flexion increased stress by 17.02% and extension decreased 66.22%. Although disc stresses changed for flexion/extension when implanted with the device, the disc stresses at the operated level for a decompressed spine deviated further from intact than the implanted case. It has been noted by Chen et al. [60] than an increase in stress is a likely cause for

the initiation of disc degeneration. Degeneration is more likely to occur after the spine is decompressed compared to insertion of the implant.

CHAPTER 5

CONCLUSION

5.1 Artificial Facet Development and FE Simulations

A finite element study is a useful technique for the investigation of the effects of replacing a facet joint. During the early stages of the design process, a finite element model is useful for determining the drawbacks and benefits of various designs. The alternative is to create prototypes and mechanically test every iteration of the design. This is a timely and cost-intensive process which is why the finite element method was chosen for this current study.

An implant was designed to mimic lumbar motion while preserving the integrity of the spine. A goal during the early stages of the development process was that the implant needed to withstand forces that are observed by facets at the lumbar level. Initial design testing suggested a conforming "ball" and "trough" design would withstand forces while transferring forces in a manner that would not lead to deformation of the components. It was the design intent that forces be transferred from the superior component to the inferior component through the "ball" and "trough" features to avoid failure due to point loads on the inferior component. When testing the implants at anatomical loading conditions, artificial boundary conditions were required to complete the analysis. Although results were insightful for the general performance of the implant design, a lumbar model was required to gather specific results and to make an improved recommendation of the implant design.

The validated lumbar spine was a valuable tool for the evaluation of facet loads, disc stresses and ROM. When the implanted model was compared to the laminectomy and facetectomy models, the artificial facet model was able to maintain motion similar to intact motion better than the decompressed models. The use of implants also maintained disc stresses similar to that of the intact model better than the models that simulated

laminectomy and facetectomy. However, when evaluating facet forces the addition of an artificial facet at the L4-L5 level increased contact forces at the adjacent level (L3-L4) by as much as 53%. This increase in forces at the adjacent level can lead to adjacent level degeneration of the facets. It is known that a change in kinematics can activate degeneration of the soft tissue surrounding the joints and lead to the need of more medical interventions.

5.2 Limitations

Several limitations exist for the current FE study. For example, certain assumptions were considered when modeling the lumbar spine. The intact facet cartilage was not explicitly modeled for the current study. The cartilage was defined as a pressure-overclosure relationship. The material property chosen was based on past finite element models of the lumbar spine. Using subject-specific material properties for the facet cartilage would lead to a more accurate model of the lumbar spine.

Only one lumbar spine model was used to test the implant. Although the implant fit in the current model, some morphological variations exist between spines of different specimens. If the implant were to be tested in multiple lumbar spines, more detailed recommendations on changes can be made to improve the design of the implant to better assist a larger market of patients.

Although the FE model was validated to literature values, no mechanical tests were performed for further validation. Experimental tests are the most direct way of obtaining kinematics of the spine and validating the FE model by ROM. Based on results of the mechanical test, adjustments can be made to each level to improve the accuracy of the overall model (L3-L5).

5.3 Future Work

The current study evaluated the implant in a short segment (L3-L5) of the spine. Although the study was able to reveal insight into the effects of the implant, a more

complete lumbar model is desired to determine the effects of the implant on the entire segment (L1-L5). The CT data that was used to create the L3-L5 also contained data for the L1 and L2 vertebrae. After segmentation of the L1 and L2, the building blocks from the inferior levels should easily map to the other vertebrae by using the same technique as previously discussed for the creation of the L4 and L5 vertebra. With the addition of the L1 and L2, the results of the implanted model may lead to a more accurate conclusion of the effectiveness of the device to better mimic the intact lumbar spine kinematics.

The results of the current study warrant a re-design of the implant. Although range of motion and disc stresses matched intact results very well, the increase in facet forces at the adjacent (L3-L4) level suggest that the implant needs to be reconstructed. It has been suggested that the use of pedicle screws in the design may help with a better fixation of the components to the bone. The apparatus that is fixated to the bone would change very little and the rod would be altered using two pieces instead of the traditional one piece. One end of each rod would then need to be designed to create a surface that articulates with the mating component. A clasped design would allow for flexion/extension. One of the implants would have additional material to help with limiting axial rotation of the two components relative to one another. A simple rendering of alterations to the mating ends of the rods is shown in Figure 71.

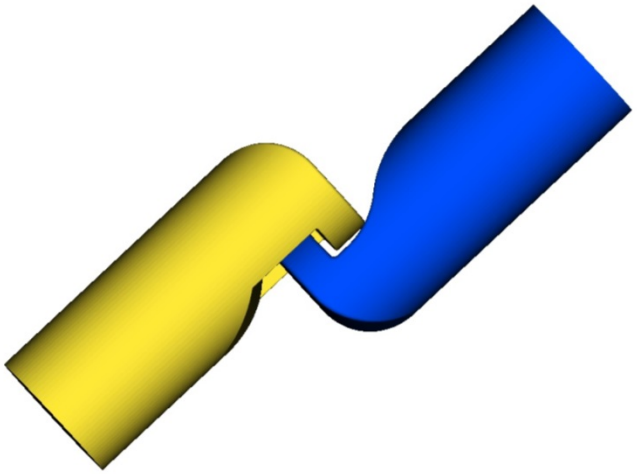

Figure 71: Redesign of rods used in pedicle screw implants.

Another area of the general design that needs development is the surgical technique and instrumentation to aid the surgeon in implanting the device. The current model was analyzed after the L4-L5 facets were removed by general approximations based on the dimensions of the components of the implant. No markers were used to determine the amount of facets to be removed. The development of instrumentation and surgical techniques that assist the surgeon in cutting and removing the appropriate amount of the articular process based on size of the facet and amount of damage would allow for quicker surgery times and reduction of surgeon errors. With a technique developed based on cadaveric trials, surgeons would be able to reproduce the surgery for multiple surgical cases with consistent results.

For the current study, testing was done solely with FE models. Development of experimental testing would further validate the models. After choosing an optimal facet replacement design based on FE results, testing should be performed to validate the design. Mechanical testing can provide insight into clinical situations that surgeons are exposed to, which may be lacking in FE models. Changes due to the addition of instrumentation are more identifiable with experimental tests. The results of the

mechanical test can lead to a design change of implant and instrumentation to improve success of the surgical outcome.

5.4 Summary Statement

The goal of this thesis was to present a new facet replacement design that would prove to be a viable option for surgeons when trying to restore the normal kinematics to eliminate further degeneration of the lumbar spine. Disc stresses and ROM were similar to intact levels; however facet forces created at the adjacent (L3-L4) level were larger than intact facet forces. With the concern of adjacent level degeneration, a re-design of the implant is necessary while maintaining the characteristics that led to a restoration of stresses and motion. The current lumbar model can be further expanded to test not only facet replacements but other advances in orthopedics for the treatment low back pain.

APPENDIX A: CONVERGENCE TEST RESULTS

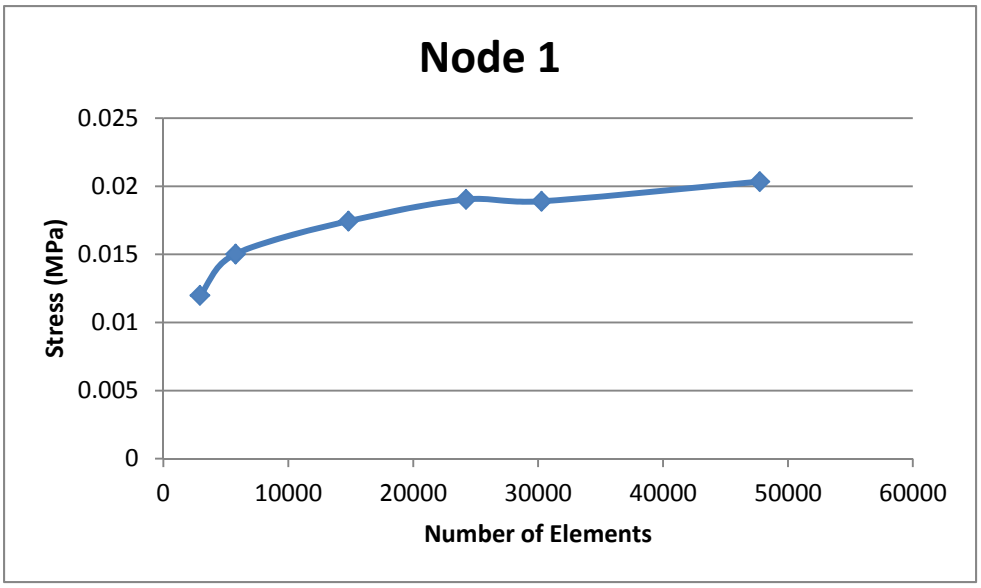

Figure A-1: Results at Node 1 for the convergence test

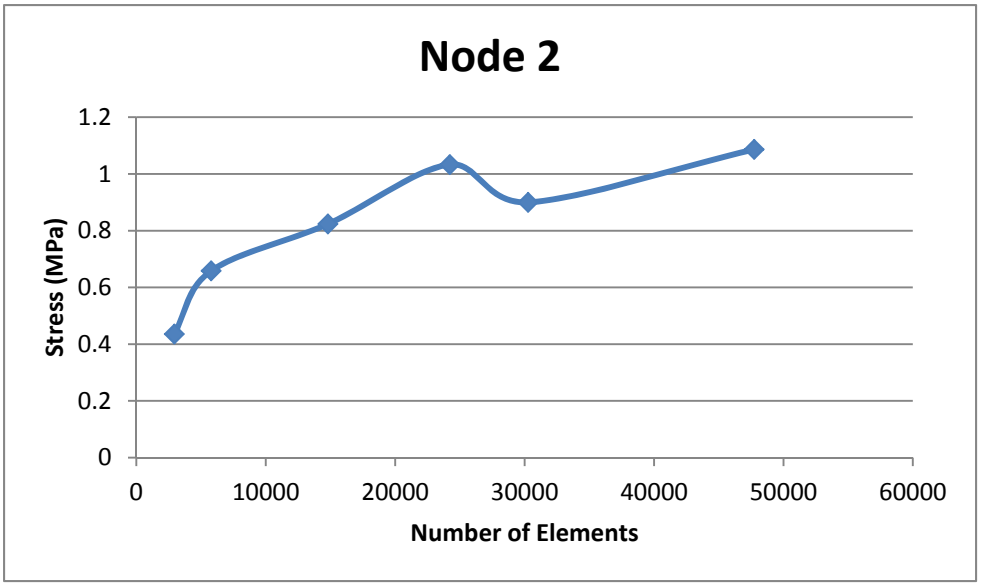

Figure A-2: Results at Node 2 for the vertebral body convergence test.

APPENDIX B: DETAILED FE ANALYSIS RESULTS

Table B-1: Motion at L3-L4 FSU for all cases.

Motion	Intact (°)	Laminectomy (°)	Facetectomy (°)	Implanted (°)
Flexion	4.038	5.583	4.264	4.095
Extension	-3.340	-3.366	-3.464	-3.498
RLB	3.225	3.247	3.336	3.167
LLB	-3.129	-3.131	-3.226	-3.040
LAR	1.868	1.977	1.850	1.771
RAR	-1.893	-1.927	-1.898	-1.782

Table B-2: Motion at L4-L5 FSU for all cases.

Motion	Intact (°)	Laminectomy (°)	Facetectomy (°)	Implanted (°)
Flexion	3.501	6.276	6.602	4.211
Extension	-6.159	-6.181	-7.412	-2.228
RLB	2.689	2.737	2.959	2.524
LLB	-2.762	-2.765	-2.941	-2.319
LAR	1.753	2.168	5.138	1.891
RAR	-2.180	-2.430	-4.944	-1.600

Table B-3: Contact forces at the left facet of the L3-L4 FSU for all cases.

Motion	Intact (N)	Laminectomy (N)	Facetectomy (N)	Implanted (N)
Flexion	0.22	0.00	4.32	4.116
Extension	64.79	66.15	63.31	89.590
RLB	0.00	0.00	0.00	0.00
LLB	8.35	8.46	9.79	11.150
LAR	0.00	0.00	0.00	0.00
RAR	159.60	159.70	161.70	175.30

Table B-4: Contact forces at the right facet of the L3-L4 FSU for all cases.

Motion	Intact (N)	Laminectomy (N)	Facetectomy (N)	Implanted (N)
Flexion	0.00	0.00	0.00	4.147
Extension	50.32	51.20	48.88	36.78
RLB	8.34	8.86	9.79	12.78
LLB	0.00	0.00	0.00	0.00
LAR	166.1	163.20	168.80	159.20
RAR	0.00	0.00	0.00	0.00

Table B-5: Contact forces at the left facet of the L4-L5 FSU for all cases.

Motion	Intact (N)	Laminectomy (N)	Implanted (N)
Flexion	3.46	0.00	66.68
Extension	65.05	59.74	204.10
RLB	0.00	0.00	0.00
LLB	39.85	38.81	89.97
LAR	0.00	0.00	0.00
RAR	168.50	153.00	199.50

Table B-6: Contact forces at the right facet of the L4-L5 FSU for all cases.

Motion	Intact (N)	Laminectomy (N)	Implanted (N)
Flexion	0.00	0.00	11.92
Extension	75.47	70.39	251.80
RLB	33.01	30.52	81.53
LLB	0.00	0.00	0.00
LAR	160.80	158.1	168.10
RAR	0.00	0.00	0.00

Table B-7: IVD von Mises stresses of the L3-L4 disc for all cases.

Motion	Intact (MPa)	Laminectomy (MPa)	Facetectomy (MPa)	Implanted (MPa)
Flexion	0.492	0.640	0.521	0.491
Extension	0.518	0.521	0.532	0.560
RLB	0.658	0.660	0.661	0.660
LLB	0.581	0.580	0.581	0.584
LAR	0.248	0.251	0.244	0.231
RAR	0.262	0.263	0.259	0.269

Table B-8: IVD von Mises stresses of the L4-L5 disc for all cases.

Motion	Intact (MPa)	Laminectomy (MPa)	Facetectomy (MPa)	Implanted (MPa)
Flexion	0.527	0.871	0.906	0.617
Extension	1.097	1.098	1.281	0.371
RLB	0.737	0.743	0.809	0.680
LLB	0.712	0.712	0.758	0.645
LAR	0.302	0.338	0.497	0.328
RAR	0.339	0.348	0.447	0.328

REFERENCES

[1] Association AC. Back Pain Facts & Statistics. Arlington: American Chiropractic Association; 2012 [cited 2012 November 11]; Available from: http://www.acatoday.org/level2_css.cfm?T1ID=13&T2ID=68.

[2] Medicine TAAoP. AAPM Facts and Figures on Pain. The American Academy of Pain Medicine; 2011 [cited 2011 October 15]; Available from: http://www.painmed.org/patient/facts.html.

[3] Goel VK, Weinstein JN. Biomechanics of the spine: clinical and surgical prospective: CRC Press; 1990.

[4] White AA, Panjabi MM. Clinical biomechanics of the spine: Lippincott Philadelphia; 1990.

[5] Cramer GD, Darby SA. Basic and Clinical Anatomy of the Spine, Spinal Cord, and ANS-E-Book: Mosby; 2005.

[6] Goel VK, Grauer JN, Patel TC, Biyani A, Sairyo K, Vishnubhotla SL, et al. Effects of charite artificial disc on the implanted and adjacent spinal segments mechanics using a hybrid testing protocol. Spine. 2005;30(24):2755.

[7] Myers ER, Wilson SE. Biomechanics of osteoporosis and vertebral fracture. Spine. 1997;22(24S):25S-31S.

[8] Natarajan R, Andersson G, Patwardhan A, Andriacchi T. Study on effect of graded facetectomy on change in lumbar motion segment torsional flexibility using three-dimensional continuum contact representation for facet joints. Journal of biomechanical engineering. 1999;121(2):215.

[9] Lee K, Teo E. Effects of laminectomy and facetectomy on the stability of the lumbar motion segment. Medical engineering & physics. 2004;26(3):183-92.

[10] Weinstein JN, Lurie JD, Olson P, Bronner KK, Fisher ES, Morgan MTS. United States trends and regional variations in lumbar spine surgery: 1992–2003. Spine. 2006;31(23):2707.

[11] Iguchi T, Kurihara A, Nakayama J, Sato K, Kurosaka M, Yamasaki K. Minimum 10-year outcome of decompressive laminectomy for degenerative lumbar spinal stenosis. Spine. 2000;25(14):1754-9.

[12] Geisler FH, Blumenthal SL, Guyer RD, McAfee PC, Regan JJ, Johnson JP, et al. Neurological complications of lumbar artificial disc replacement and comparison of clinical results with those related to lumbar arthrodesis in the literature: results of a multicenter, prospective, randomized investigational device exemption study of Charite intervertebral disc. Journal of Neurosurgery: Spine. 2004;1(2):143-54.

[13] Serhan H, Mhatre D, Defossez H, Bono CM. Motion-preserving technologies for degenerative lumbar spine: the past, present, and future horizons. SAS Journal. 2011;5(3):75-89.

[14] Demetropoulos CK, Sengupta DK, Knaub MA, Wiater BP, Abjornson C, Truumees E, et al. Biomechanical evaluation of the kinematics of the cadaver lumbar spine following disc replacement with the ProDisc-L prosthesis. Spine. 2010;35(1):26.

[15] Schmidt H, Galbusera F, Rohlmann A, Zander T, Wilke HJ. Effect of multilevel lumbar disc arthroplasty on spine kinematics and facet joint loads in flexion and extension: a finite element analysis. European Spine Journal. 2012;21:663-74.

[16] White AA, Panjabi MM. Clinical biomechanics of the spine: Lippincott Philadelphia; 1978.

[17] Fitz WR. Artificial facet joint. Google Patents; 1996.

[18] Goble EM, Fallin TW, Hoy RW. Multiple facet joint replacement. Google Patents; 2003.

[19] Reiley MA. Facet arthroplasty devices and methods. Google Patents; 2004.

[20] Goble EM, Fallin TW, Hoy RW. Facet joint replacement. Google Patents; 2006.

[21] HUDGINS RG, LANCIAL ME, HESTAD HD. FACET REPLACEMENT/SPACING AND FLEXIBLE SPINAL STABILIZATION. WO Patent 2,007,030,363; 2007.

[22] Krishna M, Friesem T. POSTERIORLY INSERTED ARTIFICIAL DISC AND AN ARTIFICIAL FACET JOINT. Google Patents; 2007.

[23] Stone MK, Suh SSH, Broman RJ, Alferness A, Finazzo AV, Charbonneau MT, et al. FACET REPLACEMENT DEVICE REMOVAL AND REVISION SYSTEMS AND METHODS. Google Patents; 2007.

[24] Zhu Q, Larson CR, Sjovold SG, Rosler DM, Keynan O, Wilson DR, et al. Biomechanical evaluation of the Total Facet Arthroplasty System™: 3-dimensional kinematics. Spine. 2007;32(1):55-62.

[25] Chin KR, Chang CA, Deros Y, Ibarra M, Turner T. DYNAMIC FACET REPLACEMENT SYSTEM. Google Patents; 2008.

[26] Kwak SKD, Borgstrom A, Lopez E, Hawkins JR, LaSota DR, Bartish Jr CM. Facet joint prosthesis. Google Patents; 2010.

[27] Link HD. Facet joint prosthesis. Google Patents; 2011.

[28] Kwak SD, Hawkins JR, Borgstrom A, Dunbar W. Artificial facet joint. Google Patents; 2011.

[29] Kuo CS, Hu HT, Lin RM, Huang KY, Lin PC, Zhong ZC, et al. Biomechanical analysis of the lumbar spine on facet joint force and intradiscal pressure-a finite element study. BMC musculoskeletal disorders. 2010;11(1):151.

[30] Cook DJ, Cheng BC. Development of a Model Based Method for Investigating Facet Articulation. Journal of biomechanical engineering. 2010;132(6).

[31] Cheng B, Gladowski D, Jegapragasan M, Cook D, Whiting D, editors. Facet Joint Complex Considerations for Biomechanics of the Lumbar Functional Spinal Unit: An Improved Model Based Method for Investigating Facet Articulation. 6th World Congress of Biomechanics (WCB 2010) August 1-6, 2010 Singapore; 2010: Springer.

[32] Sawa AGU, Crawford NR. The use of surface strain data and a neural networks solution method to determine lumbar facet joint loads during in vitro spine testing. Journal of biomechanics. 2008;41(12):2647-53.

[33] Sharma M, Langrana N, Rodriguez J. Modeling of facet articulation as a nonlinear moving contact problem: sensitivity study on lumbar facet response. Journal of biomechanical engineering. 1998;120(1):118.

[34] Wilke HJ, Schmidt H, Werner K, Schmölz W, Drumm J. Biomechanical evaluation of a new total posterior-element replacement system. Spine. 2006;31(24):2790-6.

[35] Phillips FM, Tzermiadianos MN, Voronov LI, Havey RM, Carandang G, Renner SM, et al. Effect of the Total Facet Arthroplasty System after complete laminectomy-facetectomy on the biomechanics of implanted and adjacent segments. The Spine Journal. 2009;9(1):96-102.

[36] Goel VK, Mehta A, Jangra J, Faizan A, Kiapour A, Hoy RW, et al. Anatomic facet replacement system (AFRS) restoration of lumbar segment mechanics to intact: a finite element study and in vitro cadaver investigation. SAS Journal. 2007;1(1):46-54.

[37] Panjabi MM, Henderson G, James Y, Timm JP. StabilimaxNZ® versus simulated fusion: evaluation of adjacent-level effects. European Spine Journal. 2007;16(12):2159-65.

[38] Charles YP, Persohn S, Steib JP, Mazel C, Skalli W. Influence of an auxiliary facet system on lumbar spine biomechanics. Spine. 2011;36(9):690.

[39] Meijer GJM, Homminga J, Veldhuizen AG, Verkerke GJ. Influence of Interpersonal Geometrical Variation on Spinal Motion Segment Stiffness: Implications for Patient-Specific Modeling. Spine. 2011;36(14):E929-E35.

[40] Grosland NM, Shivanna KH, Magnotta VA, Kallemeyn NA, DeVries NA, Tadepalli SC, et al. IA-FEMesh: An open-source, interactive, multiblock approach to anatomic finite element model development. Computer methods and programs in biomedicine. 2009;94(1):96-107.

[41] Collings E. Materials properties handbook: titanium alloys: ASM International (OH); 1994.

[42] Wang YQ, Li J. Sliding wear behavior and mechanism of ultra-high molecular weight polyethylene. Materials Science and Engineering: A. 1999;266(1–2):155-60.

[43] Rohlmann A, Burra NK, Zander T, Bergmann G. Comparison of the effects of bilateral posterior dynamic and rigid fixation devices on the loads in the lumbar spine: a finite element analysis. European Spine Journal. 2007;16(8):1223-31.

[44] Grosland NM. Spinal adaptations in response to interbody fusion systems: A theoretical investigation [9834465]. United States -- Iowa: The University of Iowa; 1998.

[45] Magnotta VA, Harris G, Andreasen NC, O'Leary DS, Yuh WTC, Heckel D. Structural MR image processing using the brains2 toolbox. Computerized Medical Imaging and Graphics. 2002;26(4):251-64.

[46] Andreasen NC, Cohen G, Harris G, Cizadlo T. Image processing for the study of brain structure and function: problems and programs. The Journal of neuropsychiatry and clinical neurosciences. 1992.

[47] DeVries NA, Gassman EE, Kallemeyn NA, Shivanna KH, Magnotta VA, Grosland NM. Validation of phalanx bone three-dimensional surface segmentation from computed tomography images using laser scanning. Skeletal radiology. 2008;37(1):35-42.

[48] Tadepalli SC. Patient-specific hexahedral mesh generation for orthopaedic surgical planning of cervical laminoplasty: THE UNIVERSITY OF IOWA; 2009.

[49] Kallemeyn NA, Tadepalli SC, Shivanna KH, Grosland NM. An interactive multiblock approach to meshing the spine. Computer methods and programs in biomedicine. 2009;95(3):227-35.

[50] Schmidt H, Heuer F, Simon U, Kettler A, Rohlmann A, Claes L, et al. Application of a new calibration method for a three-dimensional finite element model of a human lumbar annulus fibrosus. Clinical Biomechanics. 2006;21(4):337-44.

[51] Goel VK, Ramirez SA, Kong W, Gilbertson LG. Cancellous bone Young's modulus variation within the vertebral body of a ligamentous lumbar spine--application of bone adaptive remodeling concepts. Journal of biomechanical engineering. 1995;117(3):266.

[52] Natarajan A. Hexahedral meshing of subject-specific anatomic structures using registered building blocks. 2010.

[53] Kallemeyn NA, Natarajan A, Magnotta VA, Grosland NM. Hexahedral meshing of subject-specific anatomic structures using mapped building blocks. 2011.

[54] Vadapalli S, Sairyo K, Goel VK, Robon M, Biyani A, Khandha A, et al. Biomechanical rationale for using polyetheretherketone (PEEK) spacers for lumbar interbody fusion–a finite element study. Spine. 2006;31(26):E992.

[55] Sharma M, Langrana NA, Rodriguez J. Role of ligaments and facets in lumbar spinal stability. Spine. 1995;20(8):887.

[56] Kong W, Goel V, Gilbertson L. Prediction of biomechanical parameters in the lumbar spine during static sagittal plane lifting. Journal of biomechanical engineering. 1998;120(2):273.

[57] Rohlmann A, Zander T, Schmidt H, Wilke HJ, Bergmann G. Analysis of the influence of disc degeneration on the mechanical behaviour of a lumbar motion segment using the finite element method. Journal of biomechanics. 2006;39(13):2484-90.

[58] Kiapour A, Ambati D, Hoy RW, Goel VK. Effect of graded facetectomy on biomechanics of dynesys dynamic stabilization system. Spine. 2012;37(10):E581.

[59] Chen SH, Zhong ZC, Chen CS, Chen WJ, Hung C. Biomechanical comparison between lumbar disc arthroplasty and fusion. Medical engineering & physics. 2009;31(2):244.

[60] Chen CS, Cheng CK, Liu CL, Lo WH. Stress analysis of the disc adjacent to interbody fusion in lumbar spine. Medical engineering & physics. 2001;23(7):485-93.

[61] Dooris AP, Goel VK, Grosland NM, Gilbertson LG, Wilder DG. Load-sharing between anterior and posterior elements in a lumbar motion segment implanted with an artificial disc. Spine. 2001;26(6):E122-E9.

[62] Schmidt H, Shirazi-Adl A, Galbusera F, Wilke HJ. Response analysis of the lumbar spine during regular daily activities—A finite element analysis. Journal of biomechanics. 2010;43(10):1849-56.